Electrostatic Parameters of Ionic Crystals

M. M. Mestechkin[a)]
2875 Cowley Way, #201, San Diego, California 92110-1009

Received January 14, 2000; revised manuscript received May 15, 2000

More than 200 Madelung constants (MCs), site potentials, and electric field gradient components for ionic crystals of different nature calculated by means of the modified Madelung–Born method are presented. The same technique has helped in finding superposition rules interconnecting different classic crystals, which are useful for checking the accuracy of calculated MCs, the local site potentials, and electric field gradient tensors. The definition of Madelung interaction potentials (MIPs) is introduced, and these purely geometric quantities, independent of particular charge distribution, are found the most suitable for tabulation of crystal electric field parameters. MIPs are calculated between a number of characteristic points of fcc, bcc, hcp, and some other cells. MIPs depend strongly on the choice of cell geometric parameters but allow easy calculation of the local potentials for arbitrary point charge distribution, which are independent of this choice. The site potentials determined for yttrium ceramics, fullerides, and superfullerides make it possible to examine some regularities useful for interpretation of the observed phenomena already at the electrostatic level. The comparison of the most recent results with the calculations of MC of known crystals by means of the Evald and other techniques reveals complete agreement. The advantages of the present approach are manifested in calculations of the surface electrostatic parameters, which are found for a number of crystal planes, surfaces, and sets of layers including those composed of different crystals and those containing charged crystal planes. This technique can be applied for computation of MCs, site potentials, and electric field gradients for a crystal body restricted by two parallel planes, oriented arbitrarily to the crystal axes, in a layer situated at any depth from the surface. [S0047-2689(00)00304-4]

Key words: electric field gradient; fullerides; ionic crystal local potentials; ionic crystal surface energy; Madelung constants; Madelung interaction potentials; surface electric parameters; yttrium ceramics; zero order McDonald function.

Contents

1. Introduction. 572
2. Method. 573
3. Cubic Lattices. 575
4. Madelung Interaction Potentials. 577
5. Some Tetragonal and Other Lattices. 578
6. Fullerides. 581
7. Hexagonal Lattices. 583
8. Surface Field Parameters of Ionic Crystals. 588
9. Conclusions. 594
10. Acknowledgment. 594
11. References. 594

List of Tables

1. Electric field parameters of traditional cubic lattices. 577
2. Madelung interaction potentials of bcc lattice. . . . 579
3. Madelung interaction potentials of fcc lattice. 580
4. Electric field parameters of yttrium ceramics. 581
5. Madelung interaction potentials of $YBa_2Cu_3O_7$ ceramic. 582
6. Electric field parameters of some tetragonal and other crystals. 583
7. Electric field parameters of fcc superfullerides. . . . 584
8. Electric field parameters of bcc superfullerides. . . 585
9. Madelung interaction potentials of hcp lattice. . . . 586
10. Electric field parameters of hcp superfullerides. . . 587
11. Electric field parameters of hexagonal symmetry crystals in real geometry. 588
12. The surface electric field parameters of different crystals. 590
13. Geometric potential factors for L-system layers containing charged planes. 592
14. Potentials of charged planes in layers of some ionic crystals. 593

List of Figures

1. The charge distribution L_3. 574
2. Characteristic points of L_3 system. 575
3. "Shifting" of Cs atom to the origin. 576
4. The smooth branch of MIP in fcc elementary cell. 580
5. The local potential at Cu_1 in yttrium ceramics as a function of its formal charge. 581

a)Electronic mail: mmm3ls@ixpres.com

6. The voltage between plane and apical oxygens in yttrium ceramics as a function of Cu_1 formal charge. 582
7. Positions of trigonal vacancies (I) in the fcc crystallographic cell. 584

1. Introduction

The discovery of new high temperature superconductors, such as copper oxide ceramics and doped fullerides, as well as new magnetic organometallic compounds (all ionic crystals), has enlivened interest in the relatively old branch of the classic theory of solids: the electrostatics of ionic crystals.[1–8] In fact, each modern quantum consideration of these solids includes a preliminary calculation of the electrostatic field. The direct use of electrostatic field parameters [the best known of which is the Madelung Constant (MC)] in experimental investigations of ionic crystals includes the determination of the cohesive energy, the estimation of the shifts of ions' electronic levels in x-ray and optical spectra, the prediction of NQR frequencies, the relative stability of doped crystal modifications, and the description of the band structure and surface electronic levels, etc.

Often it seems that all problems with the classical theory of ionic crystals had been solved at the beginning of the last century in the known works of Madelung,[9] Born,[10,11] Evald,[12] Evjen,[13] and others. The most convenient parameters of electric potential in a crystal are such absolute constants as Madelung's or geometric factors of potential. However, even the most commonly used textbooks, including exhaustive editions such as Landolt–Bornstein,[14] and the latest edition of the *Handbook of Chemistry and Physics*,[15] as well as others, contain no more than 15 MCs for the simplest crystals, calculated with varying accuracy at different times.

Computer programs[1–4] for quantum mechanical calculation of ionic crystal properties are often based on the Evald method for finding MC, potentials at atomic location points, electric field gradients (EFGs), etc. The review of Tosi[16] is usually quoted in connection to this. The prevalence of the Evald method is possibly due to its thorough description in the more commonly used textbooks on the solid state theory [e.g., Kittel,[17] Huag (Appendix B),[18] and Pavinskiy[19]]. Nevertheless, other approaches are used in modern investigations. For instance, Evjen's method is often applied in calculations of EFG,[5,20] although it requires an additional evaluation of a special correcting (not small) constant[21] for many lattices. The Evjen method has been formulated as a universal way to accelerate the covergence of the Leibniz type series by Hajj,[22] who determined a very accurate value of MC for NaCl. We shall not elaborate on the history of MC calculation (a complete list of references concerned with six traditional cubic lattices can be found in Tosi's review[16]), but the competition between the Madelung–Born and Evald methods is not devoid of interest. The Madelung–Born method is based on the explicit expression for the potential of infinite periodic linear distribution of point charges in terms of the infinite sum of modified Bessel (McDonald) functions. The Evald method, containing the Fourier transformation of crystal charge distribution, is oriented on numerical calculations. Its success depends on the proper selection of an optimization constant inherent in it. In fact, the Madelung–Born expression has been deduced anew[16,23,24] while it was criticized by Hartman[25] and substituted for the modified Evald equation (in calculation of MC for CdI_2). Nevertheless, the most accurate values of MC with 15 figures have been obtained in the framework of Born's approach[26] or by direct summation of the numerical series.[22,27] It appeared that the final point was presented by Metzger,[28,29] who created convenient FORTRAN programs which apply the Evald scheme for a crystal using the results of its structure measurement directly. Yet, new efforts have been based on the framework of the Evald method.[30,31] In summary, the attempts to improve methods of the electrostatic constants calculations continue from their introduction up to recent years.[4,20–35]

This article contains MC and other electrostatic lattice parameters for a number of ionic crystals. All of these are obtained in the framework of the Madelung–Born method combined with the Evjen idea by the author.[24,33–35] In this scheme the neutral domain of the Evjen approach is infinite: it is a set of unrestricted parallel lines of alternating point charges. Although such a system itself is not a lattice of some real crystal, an arbitrary ionic crystal can be built from a definite small number of this type of domain by a simple procedure. As a result, the electrostatic potential at any point of the crystal (including, naturally, atomic positions and thus MC) can be expressed in terms of the McDonald function. The accuracy of this scheme is restricted only by the accuracy of existing interpolation expressions for the McDonald function,[36] which guarantee 5–6 accurate decimal places for MC. This accuracy is satisfactory for standard purposes. All values of MCs, vacancy potentials, and EFG tensor (obtained by differentiation of the potential formulas) mentioned in this article are calculated using this method.

On the other hand, this decomposition of any ionic lattice allows one to easily find connections between different standard lattices (such as NaCl, CsI, ZnS, Cu_2O and perovskite) in the spirit of Hund's lattice superposition rule,[37] and to express all potentials of atomic and symmetric vacant positions in terms of only three constants. A search for these types of connections has been performed earlier,[26,38] and is described in full detail in the paper of Tosi.[16] For instance, a relation between perovskite, cuprite, and CsCl lattices has been inferred,[38] but, seemingly, never proven. The proof follows automatically from the above technique. Such connections are very useful for checking the accuracy of calculated MCs. The three previously mentioned parameters can be found from the very precise calculations of MC by Sakamoto[26] for three lattices: NaCl, CsI, and Cu_2O, opening the possibility of presenting MC and atomic potential factors for all standard cubic lattices with the high accuracy of 10–15 decimals.

It is worthwhile to note that it becomes unclear whether any publication of MCs is needed at all, especially in the

light of papers such as Metzger's.[28,29] Indeed, these quantities can be immediately extracted from computer calculations for each and every new ionic crystal. Here, the situation is very similar to that with standard mathematical functions, which was reviewed by the Ad Hoc Advisory Committee (whose decisions are mentioned in the Preface to the *Handbook of Mathematical Functions*[36]). Most of these functions are packed in, e.g., the FORTRAN Library, and some simply in calculators. And yet, following the argument of the Committee and the practices of the authors of a handbook,[15] we may consider some tables of the electrostatic parameters of ionic crystals to be useful. We can approach the situation in pure mathematics even more closely by considering Madelung interaction potentials[35] (MIP). These quantities are independent either of the scaling or of the values of the point charges, and for ideal lattices, of the results of any measurements, but make it possible to easily find MC for many crystals.

More specifically, an almost incalculable number of ionic crystals makes it irrational to concentrate MCs for all of them in one place beforehand. However, if some of them are needed for consideration of a specific physical or chemical problem of one time, such as the nature of conductivity of oxides,[8] all of the necessary parameters can be calculated by means of a program. Almost 200 site potentials were presented in the aforementioned paper; 93 key quantities, the voltages (V) between metal and oxygen, have been extracted from these potentials.[8] MIP gives a much simpler possibility. For example, a single MIP 3.49513 between atomic and octagonal positions of fcc lattice (refer to Table 3) makes it possible to find the mentioned voltage for all 17 considered crystals of $Fm3n$ group. For this, it should only be expressed in Volts by transition from the cell vector length $1/\sqrt{2}$ to the distance metal–metal R (in A) and from the unit (e/A) to Volts by means of the numerical coefficient 14.4. Then $V=2*3.495*14.4*\sqrt{2}/R=142.3508/R$, (2 is the electronic charge of oxygen). Similarly, MIP 18.8334 between perovskite Bi and O makes it possible to calculate the voltage for 14 oxides of perovskite type.[8] Thus, instead of the tabulation of 62 site potentials, it is enough to have only two MIPs produced by computer; the rest can be done by "the pencil and envelope." An arbitrary charge transfer in yttrium ceramics[2] can also be treated by means of a small number of MIPs (refer to Sec. 6). Therefore, it seems that these quantities are the most suitable for tabulation.

The presented numerical data consist of a table of MCs and vacancy potentials for the ten standard lattices given with 13 decimals. All idealized lattices are assumed to have an integer ratio of lengths of cell vectors, except for the ideal hexagonal closed packing (hcp) lattice where $c/a=\sqrt{(8/3)}$. For that reason, for a number of atomic positions in cubic crystals, EFG is proved to be zero. For the rest of them, all components of EFG tensor are expressed through only two constants. The first table is the starting point for MIP calculation. The rest of the data (including EFG components) are given with 5–6 decimals, which is sufficient for all standard purposes. The MCs' tables for doped fullerides collect results for approximately 75 idealized lattices, containing alkali, alkali earth cations, and a mixture of the two in different positions. This extended number of idealized lattices is the result of a great electron affinity of fullerene, the large size of the fullerene "ball," and the resulting ability of cations to fill the "small" trigonal vacancies. All of these data can be reproduced from a much smaller number of MIPs. Similar tables are prepared for ceramics $YBa_2Cu_{3+x}O_{6+y}$ with real and idealized lattices. Other tables present 20 idealized and several real hexagonal and tetragonal lattices, the latter mainly for the sake of comparison.

A separate consideration is given for surface MC constants because the described method is highly appropriate for this particular purpose. The corresponding table illustrates results for more than 20 crystal surfaces in NaCl, CsCl, and ZnS (both sphalerite and wurtzite), $BaBiO_3$, $C_{60}K_3$, TiO_2, etc. Several tables contain the most convenient quantities of electrostatics of crystals, MIPs. Some of the aforementioned results have been previously used for description of stability, electronic nature, and superconductivity of fullerides and superfullerides.[6,7,39,40]

2. Method

Consider an arbitrary lattice, which is characterized by cell vectors $\mathbf{a}_1$, $\mathbf{a}_2$, and $\mathbf{a}_3$ with angles $\theta_{12},\theta_{13},\theta_{23}$ between them. There are n point charges Q_s in each cell. The skew angle coordinate system defined by the lattice vectors is used. The coordinates of charges are (x_s, y_s, z_s) in the zero cell. The net sum of all charges is zero.

The initial point is the expression for the potential created by two straight lines of equidistant opposite point charges ± 1 at a vacant point of the negative charge.[41] The potential of a straight line of alternating point charges ± 1 at an arbitrary point immediately follows from this.[34] This line is directed along vector $\mathbf{a}_3$, and the charge distribution has period a_3. The positive charge is at point (a, b) where the aforementioned line meets plane $(\mathbf{a}_1, \mathbf{a}_2)$, and the negative charge has distance d from it (d is measured in units of a_3, while a and b are in units of a_1 and a_2, respectively). Thus, there are two charges in each cell "above" and "below" the zero cell. The potential $S(p,q,d)/a_3$ at an arbitrary point (p, q) is a rapidly convergent series $S(p,q,d)$ of McDonald functions K_0. This potential decreases exponentially with the increase of distance p from a given line, and q is the displacement of the observation point along this line from the positive charge, and both p, q are measured in units of a_3:

$$S(p,q,d)/a_3=(F(p,q)-F(p,q-d))/a_3,$$

$$F(p,q)=4\sum_{k=1}^{\infty} K_0(2\pi kp)\cos(2\pi kq), p\neq 0,$$

$$F(0,q)=|q|^{-1}+2q^2\sum_{k=1}^{\infty}[k(k^2-q^2)]^{-1}, \qquad (1)$$

$$F(0,0)=0,\ F(0,1/2)=4\ln 2.$$

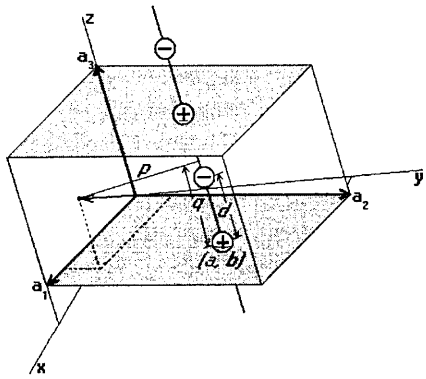

FIG. 1. The charge distribution L_3.

[See Gradstein and Ryzhik,[41] Eqs. (8.526.1), (8.361), and (0.238.1)]. In fact, $F(p,q)$ contains an additional term—$2(C+\ln(p/2))$, which is unessential until the difference $S(p,q,d)$ is used (C is the Euler constant).

Simple geometric considerations, especially clear in Fig. 1, allow the expression of distances p, q through coordinates (x, y, z) of the observation point and the lattice parameters:

$$p_n^2=x_0^2u_{11}+y_0^2u_{22}-2x_0y_0u_{12},$$

$$q_n=x_0u_1+y_0u_2+z, x_0=x-a, y_0=y-b,$$

$$u_1=(a_1\cos\theta_{13})/a_3, u_2=(a_2\cos\theta_{23})/a_3, \quad (2)$$

$$u_{12}=a_1a_2(\cos\theta_{13}\cos\theta_{23}-\cos\theta_{12})/a_3^2,$$

$$u_{11}=((a_1\sin\theta_{13})/a_3)^2, u_{22}=((a_2\sin\theta_{23})/a_3)^2.$$

Here coordinates are measured in lattice vectors units, while the final unit is a_3. Sometimes we use the Cartesian coordinate system, too. Its position, relative to the screw-angle system, is clear from Fig. 1: vectors $\mathbf{a}_1$ and $\mathbf{a}_3$ lie in the (x,z) plane with $\mathbf{a}_3$ along z axes. The latter system is connected to the crystallographic cell, while the former one is confined to the elementary cell.

We also introduce a set of similar parallel lines of charges. Each line is identified by two integers (l, m) and intersects $(\mathbf{a}_1, \mathbf{a}_2)$ plane at point $(a+l,b+m)$. Thus, there are two charges (± 1) in the same relative positions in each cell as those in the zero cell. We use the notation $L_3(a,b,d)$ for the whole set of these charges. The set of $\pm Q$ charges situated in the same points will be denoted by $QL_3(a,b,d)$. In fact a, b, d are coordinates of charge $-Q$ in each cell while those of Q are a, b, 0. Here subscript 3 refers to the direction of lines. The potential of any line (l, m) from system $L_3(a,b,d)$ is given by the same Eqs. (1) and (2) in which only a and b are replaced by $a+l$ and $b+m$, respectively. The potential of the whole set $L_3(a,b,d)$ is

$$\varphi(r)=\frac{1}{a_3}\sum_{l,m=-\infty}^{\infty} S(p_{lm},q_{lm},d). \quad (3)$$

If we add $Q_sL_3(x_s,y_s,z_s)$ to the initial lattice, we obtain the lattice in which charge Q_s is removed from its place and moved to the "bottom" of the corresponding cell. Similarly adding $Q_sL_2(0, x_s, y_s)$ and $Q_sL_1(0,0, x_s)$ to this altered lattice places charge Q_s in the origin of each cell. After application of this procedure to each charge, all of them are concentrated in the origins of cells, where they completely destroy each other, and the lattice will disappear. Thus, we would have obtained the decomposition

$$L=-\sum_s Q_s(L_3(x_s,y_s,z_s)+L_2(0, x_s,y_s)+L_1(0,0,x_s)). \quad (4)$$

Summation in Eq. (4) has taken over all charges of the zero cell of lattice L except for that of the origin of the coordinate system (if it exists). Equation (4) means that any properties of lattice L are a superposition of the corresponding properties of the set of charge distributions in the right hand part of Eq. (4). The net distribution is the set of finite dipoles, n (or n-1, if a charge is present at the origins of cells in lattice L) per each cell. The end Q_s of the dipole has coordinates r_s; the opposite charge is at the origin. In particular, the crystal potential is

$$V(r)=-\sum_s Q_s\sum_{l,m=-\infty}^{\infty}(S(p_{lm},q_{lm},z_s)/a_3 + S(p'_{lm},q'_{lm},y_s)/a_2+S(p''_{lm},q''_{lm},x_s)/a_1). \quad (5)$$

According to Eq. (4), it is necessary to substitute y for z, z for x, x for y, 0 for a, and x_s for b and simultaneously 1 for 2, 2 for 3, and 3 for 1 in the subscripts in Eq. (2) in order to calculate primed quantities. Similarly, the substitution x for z, y for x, z for y, 0 for a, 0 for b, and 1 for 3, 2 for 1, and 3 for 2 is needed for the calculation of biprimed quantities. In reality, only 15–20 terms are present in the right hand side of Eq. (5) as a result of the fast convergence. Therefore, the time for the calculation of potential is of the same order as the time for the calculation of a single McDonald function. It is clear that described procedures can be easily programmed.

The potential can be conveniently presented in a form

$$V(r)=-(e/R)\sum_{s=1}^{n} Q_s\varphi(r,r_s)=(e/R)g(r),$$

$$g(r)=-\sum_{s=1}^{n} Q_s\varphi(r,r_s), \quad (6)$$

where g is natural to mention as the geometric potential factor (GPF), and e is the absolute value of the elementary charge. R is a lattice geometrical parameter, most commonly a_3. Function $\varphi(r,r_s)$ is the internal sum in Eq. (5), with a_1, a_2, a_3 measured in units of R. In fact, $-\varphi(r,r_s)$ is the potential at r created by 1 charges with r_s relative coordinates to the corresponding cell origins where -1 charges are situated. It is a nonsymmetrical function $\varphi(r_s,r)\neq\varphi(r,r_s)$. It describes "self-interaction" $\varphi(r,r)\neq 0$ too. The latter is the potential at r in the zero cell created by unit charges with r coordinates in all of the rest of cells and by -1 charges at the origins. [The true self-interaction has been already re-

moved in Eq. (1)]. The difference $g(r,r_s)=\varphi(r,r)-\varphi(r,r_s)$ can be used in Eq. (6) instead of $\varphi(r,r_s)$ due to the zero net cell charge. The value of $g(r,r_s)$ describes the potential at point r when charges -1 are placed in all cells at the equivalent r positions, whereas charges $+1$ are situated at r_s. The "self-interaction" is excluded from $g(r,r_s)$ because $g(r,r)=0$. This function is a symmetrical at both points: $g(r,r_s)=g(r_s,r)$. The latter equality follows from the invariance to the inversion of the Bravias lattice.

We use two manners of presentation of numerical data for GPF. In ideal lattices, $g(r)$ does not depend on the results of measurements of lattice parameters. It is a dimensionless quantity, and it will be given instead of the potential value. In this case, R will be chosen as the dimension of the crystallographic cell rather than that of the elementary one. For instance, $R=a_3$ in CsCl, while $R=a_3\sqrt{2}$ in NaCl. In real crystals, $g(r)$ contains data of measurements (as well as R itself), and the lattice points' potentials are given in Volts. The same manner of representation is used for EFG: in ideal lattices it is shown as dimensionless factor ξ at e/R^3. The details of differentiation and proper definition of EFG tensor components in the skew angle coordinate system used were described earlier.[34] However, it should be mentioned that EFG could also be found by direct summation[20] of the corresponding series, which converge as reciprocal cubes in contrast to potentials and MCs, where convergence is the main problem.

Symmetric quantity $g(r,r_s)$ allows casting the electrostatic energy in the form:

$$E=(e^2/2R)\sum_{s=1}^{n} Q_s g(r_s)=(e^2/R)\sum_{1\le s<t}^{n} Q_s Q_t g(r_s,r_t)$$

$$=-e^2\alpha/R. \tag{7}$$

The first expression emphasizes the additivity of the bonding energies of different cells, while the second gives for MC a natural generalization of the known formula onto the lattice with n point charges in one cell. It resembles expression for interacting charges in which the Coulomb potential is replaced by $g(r,r_s)$

$$\alpha=-\sum_{s=1}^{n} Q_s g(r_s)/2=-\sum_{1\le s<t}^{n} Q_s Q_t g(r_s,r_t),$$

$$g(r_s)=\sum_{t=1}^{n} Q_t g(r_s,r_t). \tag{8}$$

Therefore, it is natural to mention $g(r,r_s)$ as the MIP. In contrast to the Coulomb potential, it depends not only on the distance between two points, but on their positions within the cell, and also on the lattice cell choice. It should be emphasized that MIP is a purely geometrical parameter independent of the values of lattice point charges. Therefore, the second expression allows describing charge transfer inside the crystal cell.

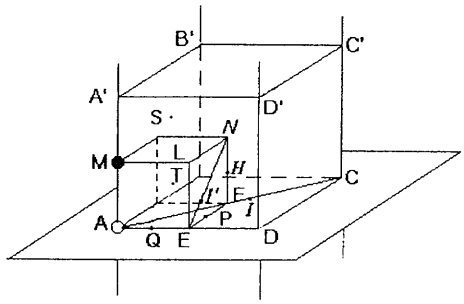

FIG. 2. Characteristic points of L_3 system.

The sign used in Eq. (8) stresses the fact that the contribution to MC from the opposite charges is positive when $g(r,r_s)$ is positive. Defining MC we must bear in mind two points: it is important not to deviate significantly from the definitions most commonly used and the fact that the real physical meaning has only the electrostatic bonding energy per cell. Elaborating the first point, we usually choose the elementary (but not crystallographic) cell as a unit. Then we obtain MC per unit chemical formula in most cases. However, to deal with the usual values for standard lattices, we use some parameter R of the crystallographic cell as the unit of length, rather than a_3. Nevertheless, to apply the same definition for two-atomic and polyatomic cells we were obligated to include charges Q_s into definition (8). Therefore, in such cases as ZnS, the usual MC is four times less than our MC.

3. Cubic Lattices

Before discussing numerical data, we will demonstrate how the above technique works. System $L_3(0,0,0.5)$ for cubic lattices is shown in Fig. 2, where certain key points are mentioned. In notation used, the unit positive charge is at A, and the negative charge is at M. According to Eqs. (1)–(3), the GPFs at A, F and E are

$$g_A\equiv a=-4\ln 2+16\sum_{k,l,m=0}^{\infty}{}' K_0(2(2k+1)\pi\sqrt{l^2+m^2})$$

$$=-4\ln 2+32(K_0(2\pi)+K_0(2\sqrt{2}\pi)$$

$$+K_0(4\pi)+2K_0(2\sqrt{5}\pi))$$

$$=-2.741366=-g_M,$$

$$g_F\equiv b=8\sum_{k=0}^{\infty}\sum_{l,m=-\infty}^{\infty} K_0(2(2k+1)\pi\sqrt{(l-1/2)^2+m^2})$$

$$=32(K_0(2\sqrt{2}\pi)+K_0(2\sqrt{2}\pi)+K_0(2\sqrt{2}\pi))$$

$$=0.219414=-g_N, \tag{9}$$

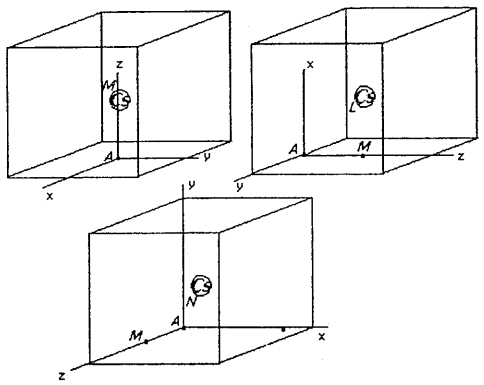

FIG. 3. "Shifting" of Cs atom to the origin.

$$g_E \equiv c = 8 \sum_{k=0}^{\infty} \sum_{l,m=-\infty}^{\infty}{}' K_0(2(2k+1)\pi \times \sqrt{(l-1/2)^2+(m-1/2)^2}) = 16(K_0(\pi)+2(K_0(\sqrt{5}\pi)+K_0(3\pi) + K_0(\sqrt{13}\pi)+K_0(\sqrt{17}\pi)) = 0.486590 = -g_L.$$

Here, the prime at the sum symbol indicates that all indices simultaneously cannot be zero. The inclusion of the rest of the terms of sums is senseless until interpolation formulas from the *Handbook*[36] are used for the McDonald function (or the corresponding program from the FORTRAN library).

Now, let us consider CsCl crystal (Fig. 3) as an example. Applying the above procedure, we begin by placing the origin of the L system at point F, with the direction to the Cs atom. This contributes $-g_M = a$ to the GPF of Cs according to Eq. (4). The next position of the origin is at E, and the direction is to F. In this case Cs occupies a position similar to that of point L in Fig. 2, and obtains the $g_L = c$ addition to the GPF. Finally, the origin coincides with the Cl atom, and the direction is from Cl to E. Now the relative position of Cs is the same as that of N relative to the origin in Fig. 2. Thus, the total GPF of Cs is $a+b+c=-2.035\,35$. It is evident that GPF of Cl is negative of the GPF of Cs, and the MC has the same absolute value. In a similar manner we obtain the whole fourth column of Table 1.

The numerical values of MCs placed in the first, fifth, and seventh rows of Table 1 are taken from Sakamoto's paper.[26] Solving equations for a, b, and c, we obtain $a=(\alpha(\mathrm{CsCl}) - \alpha(\mathrm{Cu_2O}))/3 = -2.741\,365\,174\,540\,80$, $b=(\alpha(\mathrm{Cu_2O}) - \alpha(\mathrm{NaCl}))/3 - \alpha(\mathrm{CsCl}) = 0.219\,414\,438\,483\,61$, and $c = (\alpha(\mathrm{NaCl}) - \alpha(\mathrm{CsCl})/3 = 0.486\,589\,226\,6046$. After that, we can construct the entire table. The first six decimals coincide with those in Eq. (9).

It is worthwhile to mention that the 24th and 28th rows of the table demonstrate a special property of these two lattices: the zero equipotential surfaces are planes parallel to cell faces and passing through the tetragonal vacancies.[35] These form a set of small cubes surrounding each atom. The potential is negative in small cubes containing O and positive in cubes containing Bi and Ba. It is also clear from the fourth column of Table 1 that:

$$\begin{aligned} \alpha(\mathrm{ZnS}) &= 2\alpha(\mathrm{NaCl}) + 4\alpha(\mathrm{CsCl}), \alpha(\mathrm{CaF_2}) = 4\alpha(\mathrm{CsCl}) \\ &\quad + \alpha(\mathrm{NaCl}), \\ \alpha(\mathrm{C_{60}A_3,fcc}) &= \alpha(\mathrm{NaCl}) + 4\alpha(\mathrm{CsCl}), \\ \alpha(\mathrm{C_{60}A_3,bcc}) &= 2\alpha(\mathrm{Cu_2O}) - \alpha(\mathrm{NaCl}) - 4\alpha(\mathrm{CsCl}), \\ \alpha(\mathrm{BaBiO_3}) &= 4\alpha(\mathrm{Cu_2O}) - 8\alpha(\mathrm{CsCl}). \\ \alpha(\mathrm{K_2PtCl_6}) &= 8\alpha(\mathrm{Cu_2O}) + 4\alpha(\mathrm{NaCl}) - 16\alpha(\mathrm{CsCl}). \end{aligned} \tag{10}$$

The first two equalities are discussed in Ref. 16, the fifth one was mentioned in Sec. 1; the rest are discussed in this article for the first time. The numerical value for K_2PtCl_6 is in complete agreement with the earliest calculation of Lennard-Jones and Dent.[42] Unfortunately, the second interrelation Eq. (10) reveals incorrectness (1 in the tenth figure) in the numerical value[26,38] for $\alpha(CaF_2)$. Nevertheless, we believe that the quantities used for determining of a, b, c are correct (they do not include the value for CaF_2). A model system, which may be defined as cubic Al_2O_3, is also placed in the table. It consists of four $+3$ charges in tetragonal positions and six -2 charges in the middle of all edges and faces, and may be decomposed as

$$L(\mathrm{Al_2O_3}) = L(\mathrm{Cu_2O}) + L(\mathrm{ZnS}) + L(\mathrm{BaBiO_3}). \tag{11}$$

This leads to rows 33–36 in Table 1.

This table guarantees much higher accuracy than really needed for chemical use. However, from the very beginning of the investigations on the electrostatics of ionic crystals there existed a deep interest in the exact relationships between the calculated quantities[16,22,26,38] that could separate the purely mathematical problems from the problems of physical measurements. As Johnson and Templeton, who made the first systematic computer calculation of MCs, wrote:[43] "In many cases more digits are listed than have chemical significance in order to ensure that the mathematics is not the determining factor in the accuracy with which MC is known." The high accuracy became even more important after application of the electrostatic data as a starting point in quantum calculations.

The final comment on this table is that the vertices of the mentioned small cubes in $BaBiO_3$ are the rare points from the whole table with nonzero EFG. The corresponding coefficient at e/R^3 for its component along the main cube diagonal is $\xi = 84.9638$ (the asymmetry coefficient $\eta = 0$) in the both cases (24th and 28th), the same value this coefficient holds for the Cu atom in Cu_2O. This is clear from the superposition rules Eq. (10). Using the same line of reasoning, it follows that EFG is identical for atom O in perovskite and for cation in bcc $C_{60}A_3$ ($\xi = 85.6573$, $\eta = 0$). It has half of that value ($\xi = 42.8287$) for octagonal vacancies in Cu_2O, as well as for O atoms in model Al_2O_3, and it is four times greater for Cl in K_2PtCl_6.

TABLE 1. Electric field parameters of traditional cubic lattices

Crystal	Nr	MC and GPF	Formula	Value
CsCl	1	α	$-(a+b+c)$	2.035 361 094 5260
	2	$g(\mathrm{Cl})=-g(\mathrm{Cs})$	$-(a+b+c)$	2.035 361 094 5260
	3	$g(E)=-g(F)$[1]	c	0.486 589 226 6046
	4	$G(H)$[2]		2.000 000 000 0000
NaCl	5	α	$-a-b+2c$	3.495 129 189 2664
	6	$g(\mathrm{Cl})=-g(\mathrm{Na})$	$-a-b+2c$	3.495 129 189 2664
Cu_2O	7	α	$-4a-b-c$	10.259 457 033 0750
	8	$G(\mathrm{O})$	$(-5a+b-c)/2$	6.476 530 928 9892
	9	$G(\mathrm{Cu})$	$3(a+b)/2$	−3.782 926 1040 858
	10	$g(E)=-g(F)$[1]	$-(a+3b)/2-c$	0.554 9717 029 404
ZnS	11	α	$-6(a+b)$	15.131 704 416 3431
	12	$g(S)=-g(\mathrm{Zn})$	$-3(a+b)$	7.565 852 208 1716
	13	$g(T)=-g(N)=-g(E)$[3]	$-a-b-4c$	0.575 593 829 6388
	14	$G(Q)$[4]	$2c$	0.973 178 453 2092
CaF_2	15	α	$-5(a+b)-2c$	11.636 575 227 0768
	16	$G(\mathrm{Ca})$	$3(a+b)$	−7.565 852 208 1716
	17	$g(F)$	$-2(a+b+c)$	4.070 723 018 9052
	18	$G(E)$[1]	$a+b+4c$	−0.575 593 829 6388
$BaBiO_3$	19	α	$-8(2a-b-c)$	49.509 872 1133 584
	20	$G(\mathrm{Ba})$	$2(a-2b+c)$	−5.387 209 649 8069
	21	$G(\mathrm{Bi})$	$2(2a-b-c)$	−12.377 468 028 3396
	22	$G(\mathrm{O})$	$-2a+2c$	6.455 9088 022 908
	23	$G(F)$[1]	$2b-2c$	−0.534 349 576 2420
	24	$G(T)$[3]	0	0.0
$C_{60}A_3$	25	α	$-6a+6b$	17.764 677 678 1465
(BCC)	26	$G(\mathrm{C}_{60})$	$-3a+3b$	8.882 338 839 0732
	27	$g(A_E)=g(A_F)$	$a-b$	−2.960 779 613 0244
	28	$G(T)$[3]	0	0.0
$C_{60}A_3$	29	α	$-4(2a+2b-c)$	22.121 962 794 8759
(FCC)	30	$G(\mathrm{C}_{60})$	$-2(2a+2b-c)$	11.060 981 397 4379
	31	$g(A_E)=g(A_N)$[5]	$-6c$	−2.919 535 359 6275
	32	$g(A_T)$[5]	$2(a+b+c)$	−4.070 723 018 9052
Model	33	α	$-24a-21b-9c$	56.805 757 941 3821
Al_2O_3	34	$G(\mathrm{Al})$	$9(a+b)/2$	−11.348 778 312 2574
	35	$g(\mathrm{O}_E)=g(\mathrm{O}_F)$	$-(7a+5b+6c)/2$	7.586 474 334 8700
	36	$g(A)=g(N)$[1]	$-3(a+3b+2c)/3$	1.664 915 108 8212
K_2PtCl_6	37	α	$4(-5a+b+4c)$	63.490 388 870 4239
	38	$G(\mathrm{K})$	$2(a-2b+c)$	−5.387 209 649 8069
	39	$G(\mathrm{Pt})$	$6(a-c)$	−19.367 726 406 8723
	40	$G(\mathrm{Cl})$	$-2(a-c)$	6.455 908 802 2908

[1]Octagonal vacancy. Letters correspond to Fig. 2.
[2]Vacancy. Letters correspond to Fig. 2. This is a rare point with the integer value of GPF. The first six zeros are calculated, the remaining zeros are a still unproved hypothesis (See Ref. 24).
[3]Tetragonal vacancy. Letters correspond to Fig. 2.
[4]Vacancy. Letters correspond to Fig. 2.
[5]Subscripts correspond to Fig. 2.

4. Madelung Interaction Potentials

It is also beneficial to observe the way MIPs work in ideal cubic lattices. The fcc lattice cell contains four "atomic" positions A with equal distances between them, four mutually equidistant octagonal O positions (at the center of the cell and at the middle of the edges), and eight tetragonal T positions (points T, S, etc. in Fig. 2) with three possible

mutual distances. Accordingly, there exist three MIPs $g_{AA}=g_{OO}=g_{TT''}=-a-c=2.254\,776$, $g_{TT'}=g_{AO'}=-a=2.741\,365$, $g_{TT'''}=g_{AO}=-a-b-c=2.035\,362$. The last MIP between the tetragonal positions and other positions is independent of their mutual distances and can be expressed through the former three: $g_{AT}=g_{OT}=3(g_{TT'}+g_{TT''}+g_{TT'''})/8=2.636\,813$. Generally, the MIP is reduced with the distance between the corresponding points until the distance is smaller than half the main cube diagonal. Then the MIPs begin to repeat due to the symmetry requirements. The MIP is the same for different types of points if the distances between them are equal and small enough.

Now we can calculate the GPF and MC for an ideal cubic crystal composed of arbitrary point charges with a net sum of zero situated in the aforementioned positions. For example, in a perovskite crystal $g_{Bi}=3g_{AO}Q_O+g_{AO}Q_{Ba}=3Q_O(g_{AO}-g_{AO})-Q_{Bi}g_{AO}=2.118Q_O-2.035Q_{Bi}$, and $g_O=2g_{AA}Q_O+g_{AO}Q_{Bi}+g_{AA}Q_{Ba}=-g_{AA}Q_O+Q_{Bi}(g_{AO}-g_{AA})=-2.255Q_O+0.487Q_{Bi}$. These relations proved to be useful for describing formation of hole on the oxygen lone pair band in $BaBiO_3$.[44] Naturally, for $Q_O=-2$, $Q_{Bi}=4$, we obtain the above result from Table 1. Similarly for CaF_2 we have: $g_{Ca}=3Q_{Ca}g_{AA}+8Q_Fg_{AT}=Q_{Ca}(3g_{AA}-4g_{AT})=3Q_{Ca}(a+b)/2=-3.782\,93Q_{Ca}$. In this manner, we can reproduce the entire Table 1.

We must bear in mind that MIPs depend largely on the choice of the crystal cell. For instance, let us consider the fcc elementary cell. Here, cell vectors are directed to the face centers. It contains only one point A (the origin), one point O (1/2,1/2,1/2), and two points T (1/4,1/4,1/4), (3/4,3/4,3/4), where the values in brackets are screw-angled coordinates. Therefore, the number of interactions is considerably less: $V_{AO}=V_{TT}=3.495\,13$, $V_{AT}=V_{AT'}=V_{OT}=V_{OT}=3.782\,93$. (The connection with previous quantities is self-evident; the letter V is used instead of g to avoid confusion with the aforementioned interactions between similar points in the crystallographic cell). Although the values of MIPs have been changed, the peculiarities, mentioned above remain the same, and these new values naturally lead to the same results for MC, GPF, and EFG. In particular, the value of the GPF in CaF_2 is not changed: $g_{Ca}=2Q_FV_{AT}=-Q_{Ca}V_{AT}=-3.782\,93Q_{Ca}$.

In the bcc elementary cell, the basis vectors connect the origin with the centers of three adjacent cubes. The angles formed between them are 109.°4712. The cell contains one point A (origin), three points O (cube edge centers), six points P (see Fig. 2), which are the tetragonal vacancies in the bcc lattice, six points I, and six I' etc. The last two types are trigonal vacancies of the bcc lattice; their coordinates are given in Table 2.

As a reminder, the origin of these terms is connected with the picture of the lattice that is built of spheres centered at points A. Each term reflects the number of adjacent spheres which can be touched simultaneously by a smaller sphere centered at the corresponding point. Therefore, each vacancy is characterized by its radius, e.g., for T vacancy it is $(\sqrt{15})/3-1$ in units of the main sphere radius, etc. Table 2 contains all MIPs for the bcc lattice. Similar data for the fcc lattice are located in Table 3.

We see that the MIP depends not only on the distance between corresponding points but also on their positions relative to the lattice framework, and the mentioned peculiarities of the MIP generally remain true. A smooth branch of MIP dependence on the distance can be extracted at small distances within the cell. The MIP decreases steadily until the distance slightly exceeds half of the cube edge length. When the point approaches to charges in adjacent cells, MIP begins to repeat due to symmetry requirements and loses the visible regular behavior as a function of the distance only. Therefore the same value appears for different distances and for different point types, and on the other hand, different MIP begin to correspond to the same distance depending on the point position in the cell, as in the case of $g_{1,21}$ and $g_{2,14}$. The difference between MIP and the Coulomb potential approaches zero for the smallest distances. The smooth behavior of MIP in the fcc elementary cell is demonstrated in Fig. 4.

In total, there are only nine interaction constants in the bcc cell, which make it possible to obtain MC for arbitrary point charge distribution among 44 mentioned symmetry points in the crystallographic cell of this type of ideal crystal. This ratio, 48:9, is even larger in the fcc lattice. In fact, Tables 2 and 3, contain the whole electrostatics of a crystal. The discussed tables are built by means of a modified computer program[35] (it takes a few seconds on the PC for several dozens of points). Further discussion of Tables 2 and 3 will be given below in connection with MCs of fullerides.

A similar additive approach is also possible for EFG, but here the superposition of different pair interactions requires the rather cumbersome addition of tensor quantities, which must be brought to a common coordinate system for all points' pairs beforehand, and suitable tables are not given here. Instead, we prefer to use the above-mentioned program[34] directly to the whole crystal. However, for most of the other lattices, the result depends on the measured lattice parameters, and below we give some examples to show how to apply these procedures[34] to arbitrary ionic crystals.

5. Some Tetragonal and Other Lattices

The interesting examples of tetragonal symmetry crystals are yttrium superconducting ceramics shown in Table 4. Most of them are envisioned as being constructed of cubes of identical dimensions for the sake of mutual comparison. It means that we assume $a=b=c/3$ for $YBa_2Cu_3O_6$, $YBa_2Cu_3O_7$, $YBa_2Cu_4O_8$, with the common $a=3.8422$ A for all three crystals. The same value is used for $YBa_2Cu_3O_{6.5}$, which means that for the latter two lattices elementary cell parameters are $a_1=a_2=a$, $a_3=5a/\sqrt{2}$, $\theta_{12}=\theta_{13}=90°$, $\tan\theta_{23}=7$ and $a_1=2a$, $a_2=a\sqrt{2}$, $a_3=3a$, $\theta_{12}=45°$, $\theta_{13}=\theta_{23}=90°$, respectively. The description of the structure of these crystals and notation of atomic positions are taken from Blaha,[45] where EFG for these crystals has been calculated for continuous distribution of electron density directly from the

TABLE 2. Madelung interaction potentials of bcc lattice[1]

Points	*A*	*O*	*P*	*I*
A		$g_{1,2}=2.960\,78$	$g_{1,5}=2.93143$	$g_{1,11}=g_{1,21}=2.959\,82$
O	$R_{12}=1/2$	$g_{2,3}=2.960\,78$ $r_{2,3}=(\sqrt{2})/2$	$g_{2,6}=g_{2,9}=4.2511$, 0, $g_{2,5}=2.93143$	$g_{2,11}=g_{2,14}=5.788\,25$ $g_{2,12}=g_{2,15}=$ $g_{2,21}=3.143\,84$
P	$r_{1,5}$ $=(\sqrt{5})/4$	$r_{2,6}=1/4, r_{2,9}$ $=3/4;$ $r_{2,5}=(\sqrt{5})/4.$	$g_{5,6}=$ $g_{5,7}=3.34797$ $r_{5,7}=r_{5,6}\sqrt{3}$ $=(\sqrt{6})/4$	$g_{5,11}=g_{5,20}=3.080\,26$
I	$r_{1,11}=3(\sqrt{2})/8.$ $r_{1,21}=(\sqrt{34})/8$	$r_{2,11}=(\sqrt{2})/8,$ $r_{2,14}=(\sqrt{34})/8;$ $r_{2,12}=(\sqrt{26})/8,$ $r_{2,15}=(\sqrt{10})/8,$ $r_{2,21}=(\sqrt{42})/8.$	$r_{5,11}=(\sqrt{14})/8,$ $r_{5,20}=(\sqrt{30})/8$	$g_{18,19}=2.959\,82,$ $g_{11,15}=g_{11,18}=g_{18,20}=$ $3.667\,53$ $r_{18,19}=5(\sqrt{2})/8,$ $r_{11,15}=(\sqrt{6})/8,$ $r_{11,18}=(\sqrt{22})/8,$ $r_{18,20}=(\sqrt{38})/8$
Vac. Radii	1.0000	$2(\sqrt{3})/3-1$ $=0.15470$	$(\sqrt{15})/3-1$ $=0.29099$	$(\sqrt{6})/2-1=0.224\,74$
Points' numbers and coordinates	1. 0, 0, 0	2. $\frac{1}{2}, \frac{1}{2}, 0$ 3. $\frac{1}{2}, 0, \frac{1}{2}$ 4. $0, \frac{1}{2}, \frac{1}{2}$	5. $\frac{3}{4}, \frac{1}{4}, \frac{1}{2}$ 6. $\frac{3}{4}, \frac{1}{2}, \frac{1}{4}$ 7. $\frac{1}{2}, \frac{3}{4}, \frac{1}{4}$ 8. $\frac{1}{4}, \frac{3}{4}, \frac{1}{2}$ 9. $\frac{1}{4}, \frac{1}{2}, \frac{3}{4}$ 10. $\frac{1}{2}, \frac{1}{4}, \frac{3}{4}$	11. 5/8,5/8,1/4 12. 5/8,1/4,5/8 13. 1/4,5/8,5/8 14. 3/8,3/8,3/4 15. 3/8,3/4,3/8 16. 3/4,3/8,3/8 17. 5/8,3/8,0 18. 5/8,0,3/8 19. 0,5/8,3/8 20. 3/8,5/8,0 21. 3/8,0,5/8 22. 0,3/8,5/8

[1]The upper right part of the table contains all possible MIPs between characteristic points of the bcc elementary cell (Fig. 2). The numbers of some typical points are also shown. The lower left portion gives all possible corresponding distances. The diagonal of the table include both types of parameters (if the suitable set of points consists of more than one point.) Points' coordinates are given in the elementary cell skew angled coordinate system.

Poisson equation corresponding to that density. In general, the correspondence between EFG of continuous and point charge distribution is rather poor.

Several linear dependencies are noticeable in Table 4. The first one is, in fact, a direct consequence of the charge conservation. It connects the valence of the Cu_1 atom to the oxygen contents in the crystal. The almost exact proportionality (with coefficient ≈ -10) between this valence and the crystal potential at Cu_1 is much more interesting (see Fig. 5). At the same time, potentials at ions, keeping their charges, almost never vary. O'Keeffe,[2] who postulated the consistency between the local crystal potential and the charge of copper ion in ceramic $YBa_2Cu_3O_7$, has performed a search of these types of dependencies. MIPs are very useful for such purposes because the set of MIPs allows finding the electric field for arbitrary point charge distribution. All necessary MIPs for $YBa_2Cu_3O_7$ are presented in Table 5. As an example, we extract from Table 5 expressions for potentials of all ions as a function of charges on copper ions. If Q is the value of the charge transfer from Cu_1 to Cu_2, we must add $-16.5212Q$, $6.1050Q$, $3.4225Q$, $-3.4487Q$, $23.8863Q$, $-15.1621Q$, $-15.0658Q$, and $11.4868Q$, respectively, to the suitable potentials of Y, Ba, Cu_1, Cu_2, O_1, O_2, O_3, O_4 in Table 4. The entire table of potentials from O'Keeffe[2] can be reproduced in this manner.

The most important regularity, which is clear from Table 4, is the linear dependence of the voltage between O_2 (O_3) and O_4 on the oxygen content in the crystal. The voltage passes, in fact, through zero just at a point (6.5) corresponding to the disappearance of superconductivity (see Fig. 6). This is naturally to connect to the appearance of holes in O atoms on the CuO plane. All mentioned trends are expressed even more distinctly for the real geometry of these crystals. (Suitable data are also presented in Table 4.) In real crystals, an additional feature appears, which supports the given interpretation: in the last two ceramics, the potential at the Cu_1 ion is lower than the linear dependence requires. Most likely, this potential is insufficient to hold the holes at copper. Therefore they flow to oxygen ions. The positive voltage between O_4 and O_2, which appears simultaneously with

TABLE 3. Madelung interaction potentials of fcc lattice[1]

Points	*A*	*O*	*T*	*I*
A		$g_{1,2}=3.495\ 13$	$g_{1,3}=3.782\ 93$	$g_{1,5}=3.811\ 84=g_{1,6}=g_{1,9}=g_{1,10}$
O	$r_{12}=(\sqrt{3})/2$		$g_{2,3}=g_{2,4}=3.7829\ 3$	$g_{2,5}=g_{2,6}=g_{2,9}=g_{2,10}=4.170\ 92$
T	$r_{1,4}=3(\sqrt{3})/4$	$r_{2,5}=(\sqrt{3})/4$	$g_{3,4}=3.495\ 13$	$g_{3,5}=g_{3,6}=g_{4,10}=7.104\ 49$
I	$r_{1,3}=(\sqrt{3})/4$ $r_{1,9}=2(\sqrt{3})/3=2r_{1,5}$, $r_{1,10}=2(\sqrt{6})/6=2r_{1,6}$	$r_{2,5}=(\sqrt{3})/6$, $r_{2,6}=1/2$	$r_{3,4}=(\sqrt{3})/2$ $r_{3,5}=(\sqrt{3})/12$, $r_{4,10}=(\sqrt{51})/12$; $r_{3,10}=3r_{3,5}$, $r_{3,9}=5r_{3,5}$ $r_{4,6}=(\sqrt{123})/12$	$g_{3,9}=g_{3,10}=g_{4,6}=3.640\ 39$ $g_{5,6}=4.721\ 74=g_{9,10}$ $g_{5,9}=3.811\ 84=g_{6,10}$ $g_{5,10}=3.813\ 53=g_{6,9}=g_{6,11}$ $r_{9,10}=2r_{5,6}=(\sqrt{2})/6$; $r_{5,9}=r_{1,5}$, $r_{6,10}=r_{1,6}$ $r_{6,9}=(\sqrt{22})/6$, $r_{6,11}=(\sqrt{10})/6$, $r_{5,10}=1/3$
Vac. rad	1.0000	$\sqrt{2}-1=0.4142$	0.224 74	0.154 70
Points' numbers and coordin.	1. 0,0,0	2. $\frac{1}{2}, \frac{1}{2}, \frac{1}{2}$	3.1/4, 1/4, $\frac{1}{4}$ 4.3/4, 3/4, $\frac{3}{4}$	5. 1/3,1/3,1/3 9. 2/3,2/3,2/3 6. 0,1/3,1/3 10. 0,2/3,2/3 7. 1/3,0,1/3 11. 2/3,0,2/3 8. 1/3,1/3,0 12. 12. 2/3,2/3,0

[1]The upper right portion of the table contains all possible MIPs between characteristic points of the fcc elementary cell (Fig. 2). The numbers of some typical points are also shown. The lower left part gives all possible corresponding distances. The diagonal of the table include both types of parameters (if the suitable set of points consists of more than one point.) Points' coordinates are given in elementary cell skew angled coordinate system.

these holes, means that holes are directed only to oxygen ions in the CuO plane. In other words, the narrow bands of oxygen lone pairs are not completely filled, which is a necessary requirement for the existence of large electron pair states occupation numbers, i.e., pair condensation and, thus, superconductivity.[44]

The values from Table 6 for the crystals that were considered by Templeton[43] completely confirm the results of this first application of electronic computers to calculation of MCs. The data for hexagonal type crystals, discussed below, lead to the same conclusion. At the same time, comparison with tables from the textbooks[14,15] reveals some deviations from the table of Templeton,[43] as well as from the present calculations. The table from the *Handbook*,[15] even in the latest edition (1999), in fact, reproduces on p. 12-36 (in different scale) the collection of the oldest results.[14] It is also necessary to mention that presentation of data for nonideal crystals is justified only if the values of geometric lattice parameters used are given simultaneously. Therefore, we restrict ourselves by checking some of the known results.[8,43] These MCs, together with some new data for tetragonal and other crystals, are reproduced in Table 6.

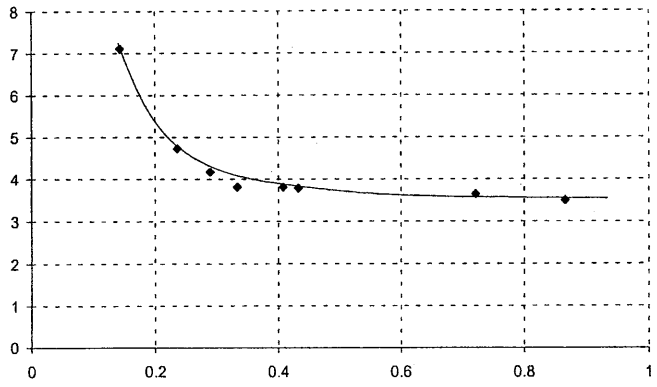

FIG. 4. The smooth branch of MIP in fcc elementary cell.

The discussion after Table 4 has shown the usefulness of idealization of crystal geometry: simplifications rarely influence conclusions, which follow from the electrostatic consideration. The situation remains the same for TiO_2 type crystals, too. Here we can assume that all distances metal–oxygen are equal. This assumption permits one to express the additional structure parameter x (which sometimes is unknown) through the ratio $u=a_3/a_1$ of the lattice constants: $x=(1+u^2/2)4$.

The values of MCs for TiO_2 and MgF_2 after transition to the shortest anion–cation distance scale are equal to 19.0802 and 4.7621, respectively, and coincide exactly with results of Templeton.[43] The second entries for TiO_2 and MgF_2 in Table 6 demonstrate that the change in calculated parameters caused by this simplification are unlikely to alter the conclusions, which are meaningful at the electrostatic level. The third entry for TiO_2 permits one to compare the changes caused by idealization with those resulting from the further refinement of lattice parameter measurement.

The rest of this type of oxide, included in Table 6, confirm

TABLE 4. Electric field parameters of yttrium ceramics

	$YBa_2Cu_3O_6$		$YBa_2Cu_3O_{6.5}$			$Yba_2Cu_3O_7$			$YBa_2Cu_4O_8$		
	V[1]	ζ[2]	V[1]	ζ[2]	η	V[1]	ζ[2]	η	V[1]	ζ[2]	η
Y[3]	−23.242	−6.421	−23.245	−6.427	0.0010	−23.247	−6.433	0.0020	−24.648	−6.430	0.0019
	−30.704	−1.634	−30.837	−1.811	0.0027	−33.337	−1.112	0.6510	−34.036	−1.211	0.0139
Ba	−20.011	3.210	−20.421	2.663	0.619	−20.831	−2.705	0.565	−22.033	−2.793	0.766
	−17.617	1.967	−17.967	2.069	0.679	−17.253	−1.658	0.526	−18.245	−1.564	0.848
Cu_1	−9.965	−17.166	−20.301	−3.530	0.836	−30.637	16.252	0.217	−24.027	13.441	0.205
	−12.736	−19.041	−23.000	−15.367	0.737	−29.666	16.380	0.342	−24.980	14.063	0.380
Cu_2	−29.963	8.583	−29.932	8.739	0.016	−29.901	8.865	0.017	−31.315	8.729	0.016
	−26.918	10.499	−27.097	10.888	0.005	−28.926	9.558	0.135	−29.899	9.520	0.051
O_1	-	-	21.903	−10.334	0.940	26.184	17.159	0.550	29.044	10.598	0.495
	-	-	19.601	9.878	0.757	26.885	16.312	0.416	28.585	9.008	0.954
O_2	18.703	5.881[4]	18.729	5.889	0.857	18.754	5.896	0.877	17.350	5.882	0.876
	20.799	6.080[6]	20.915	6.254	0.000	18.914	6.285	0.018	18.059	5.964	0.043
O_3	18.703	5.881[4]	18.926[5]	5.792	0.921	18.641	6.047	0.781	17.243	6.025	0.784
	20.799	6.080[6]	21.003[7]	6.198	0.026	18.821	5.104	0.065	17.997	5.495	0.036
O_4	17.818	6.021	18.729	12.387	0.383	19.639	12.550	0.263	17.884	11.283	0.277
	19.737	2.425	20.985	11.076	0.587	23.329	10.049	0.330	21.801	8.613	0.303
MC	66.772		74.467			86.063			97.866		
	70.932		78.594			89.174			102.630		
E[8]	250.242		279.083			322.541			366.776		
	264.164		294.718			335.874			382.673		

[1]The potential (in V).
[2]The main component of EFG (in 10^{20} V/m^2). The absence of the corresponding column means that asymmetry coefficient $\eta=0$.
[3]The first row for each entry corresponds to the idealized lattices ($R=3.842\,2$ A). The second row for each entry corresponds to the lattices with real geometry taken from the same sources that have been used in Ambrosh–Droxl *et al.*(Ref. 45) That means: $a_1=a_2=3.8665$, $a_3=3.073\,12a_1$ for $YBa_2Cu_3O_6$; $a_1=a_2=3.8665\sqrt{2}$, $a_3=3.094\,32a_1$ for $YBa_2Cu_3O_{6.5}$; $a_1=3.8231$, $a_2=1.016\,56a_1$, $a_3=3.055\,30a_1$ for $YBa_2Cu_3O_7$; $a_1=3.8393$, $a_2=1.008\,33a_1$, $a_3=3.542\,77a_1$ for $YBa_2Cu_3O_7$.
[4]For these ions $\eta=0.836$.
[5]For the second O_3' ion $V=18.419$, $\zeta=6.136$, $\eta=0.701$.
[6]For these ions $\eta=0.049$.
[7]For the second O_3' ion $V=21.003$, $\zeta=6.360$, $\eta=0.063$.
[8]The total cell electrostatic energy in eV.

the assertion: the difference in calculated potentials with the data from Torrance[8] does not exceed 0.1%, where a somewhat ambiguous procedure has been used for determination of x. It is worth noting that for cassiterite (SnO_2), for which the most accurate experimental data are available, the idealized value for u differs from the measured one by less than half of the last experimental figure. The results for La_2CuO_4 and for $LaSrCuO_4$ (if we put $x=0$, and $x=1$, respectively, in the last entries of Table 6) are also in reasonable agreement with published calculations.[1,8]

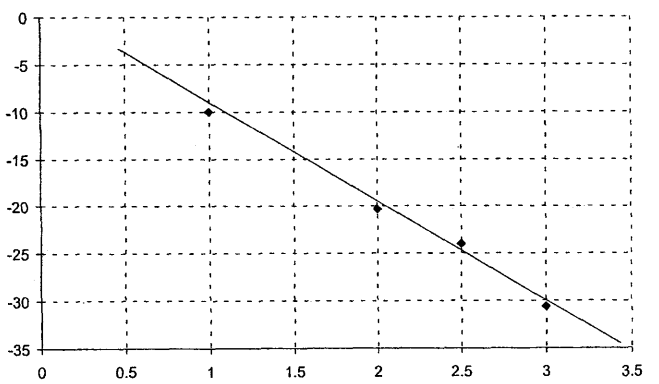

FIG. 5. The local potential at Cu_1 in yttrium ceramics as a function of its formal charge.

6. Fullerides

Fullrides and superfullerides are considered to be ideal ionic crystals. Two examples have already been included in Table 1, and two others of the tetragonal type are shown in Table 6. Both types of these ionic crystals are obtained from fullerite crystals by means of doping by alkali or alkali–earth ions.[3,46–51] The difference between these two types of crystals is in the ionic charge of the fullerene anion, which does not exceed 6 in the first case, while in the second it varies from 7 to 12. In the other words, the t_{1u} band of fullerene is being filled in fullerides, and the occupation of the next t_{2g} band begins in superfullerides. From the viewpoint of the crystal structure, their difference lies in the filling of trigonal vacancies (I).

The general definition of these vacancies follows from the same condition already mentioned in Sec. 3 for the bcc lattice: a small sphere with the center at I touches three adjacent fullerene spheres simultaneously. Trigonal vacancies (I)[40] for fcc crystals are points that lie on the segments, connecting tetragonal T and octagonal O vacancies, and di-

TABLE 5. Madelung interaction potentials of $YBa_2Cu_3O_7$ ceramic[1]

	Y	Ba	Cu_1	Cu_2	O_1	O_2	O_3	O_4
Y	-	−1.5149	−3.2145	10.0922	−3.2122	13.1175	13.4167	−2.8982
Ba	−0.7575	−1.9702	3.5049	0.9048	3.8260	0.4806	0.4563	6.9191
Cu_1	−3.2145	7.0098	-	−3.4226	10.2121	−4.2822	−4.3408	12.0094
Cu_2	5.0461	0.9048	−1.7113	0.0262	−1.7311	10.8798	10.7249	0.5227
O_1	−3.2122	7.6520	10.2121	−3.4622	-	−4.3052	−4.3154	9.8678
O_2	6.5588	0.4736	−2.1411	10.8798	−2.1526	1.5534	9.8604	−0.7311
O_3	6.7083	0.4563	−2.1704	10.7249	−2.1577	9.8604	1.6802	−0.8052
O_4	−1.4491	6.9191	6.0047	0.5227	4.9339	−0.7311	−0.8052	−0.7870

[1]The table is not completely symmetric since the interaction potentials presented account for interaction of the given ion with both symmetrical ions of identical charges (for convenience). The diagonal elements describe mutual interaction of ions of the symmetric pair. Calculated MIPs (in V) correspond to the same real geometry of $YBa_2Cu_3O_7$ that has been used in Table 4.

vide the distance TO as 1:2 (Fig. 7). Then the two points I lie on a straight line connecting the face center (F) with the cube vertex that does not belong to the mentioned face and divide this segment into three equal parts. Simultaneously, I points are centers of equilateral triangles with one vertex coinciding with that of the cube vertex and two others with two adjacent face centers. Points I touch three fullerene spheres, being at the smallest distance, $1/\sqrt{6}$ from all of them. The ratio of the radius of this cavity to that of fullerene sphere is $2/\sqrt{3}-1$, while the similar ratios for O and T vacancies are $\sqrt{2}-1$ and $(\sqrt{6})/2-1$, respectively. Thus, each T vacancy is surrounded by four I points. There are eight I vacancies in each fcc elementary cell. Their coordinates are given in Table 3. We also mention some properties of characteristic points of the bcc crystal. In this lattice O vacancies lie on the middles of the edges and faces. T vacancies (P on Fig. 2) are on the middles of the segments connecting two adjacent O vacancies. Positions of trigonal vacancies are on the face diagonals 1/8 of its length from O points, and on the same distances from the latter inside the cube body on the intersection of the equatorial plane of the cube with its diagonal plane (Fig. 2). There are three O, six T, and twelve I vacancies in a bcc elementary cell. Trigonal vacancies I lie in planes passing through centers of three adjacent fullerene spheres on equal distances $3(\sqrt{2})/8$ from them. Hence, the radii of these cavities are $(\sqrt{6})/2-1$, while those of T and O cavities, in units of the fullerene radius, are $(\sqrt{15})/3-1$ and $2/\sqrt{3}-1$, respectively. It is worth mentioning that radii of smaller vacancies remain the same, as in the fcc lattice. In principle, all electrostatic parameters of these species can be extracted from Tables 2 and 3.

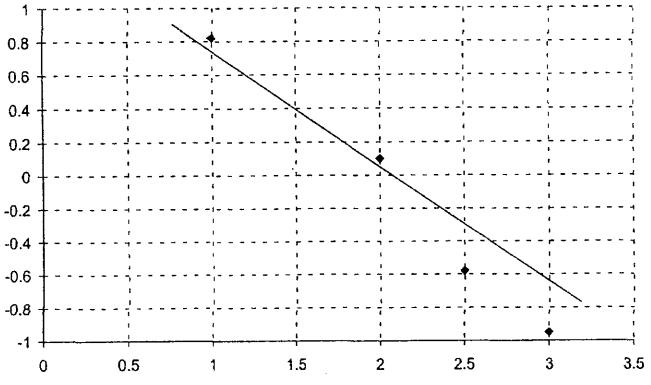

FIG. 6. The voltage between plane and apical oxygens in yttrium ceramics as a function of Cu_1 formal charge.

The first publication of MC for some fullerides was Fleming.[3] Similar data for superfullerides were presented later[6,39,40] and used for interpretation of the stability, superconductivity, and kinetics of the doping process of these compounds.[7] These parameters are shown in Table 7 for fcc and in Table 8 for bcc crystals. The EFG data from these tables are presented for the first time in this article. We can observe the connection between the values from Tables 7 and 8 and Tables 2 and 3. For instance, the MC of $C_{60}^{-11}A_{11}$ (14 line, Table 7) is according, to Eq. (8), $-4.721\,737*12 + 3.811\,835*(88-4) - 3.813\,527*12 - 7.104\,491*12 - 3.640\,389*12 + 3.495\,129*(11-1) - 4.170\,918*8 + 3.782\,926*(22-2) = 209.054\,398$, etc. Comparison of rows 4 and 5 (11 and 12, etc.) and also 6 and 7 in Table 7 shows that tetragonal positions do not feel the occupation of the octagonal positions, and anions do not "react" to the interchanging of filled and empty tetragonal positions. The explanation of these peculiarities is very simple: according to Table 3, MIPs of T points with A and O are identical. The charges at O positions completely shield the T points from the effect of the increase of A−charges as a result of this identity. Because of MIP $g_{AT} > g_{AO}$, the shift of the charge from O to T increases MC and cell electrostatic energy. The tetragonal vacancies are the closest to trigonal ones according to the definition of the latter, and this is the reason for the drastic difference (of order 15) in the GPF of T positions surrounded by I charges and not surrounded (rows 5 and 8). A similar reasoning explains the opposite change of MC and EFG for identical anionic charges (rows 5–7 and 26–28).

The results for bcc structure $A15$ used for the description[3] of $C_{60}A_3$ are shown in the 4th column of Table 8. The data for similar structures with I positions filled are collected in columns 9 and 10. The flaky structure for $C_{60}A_4$ first appeared in Fleming[3] as well. Its parameters are placed in column 5. As is clear from comparison of this column with the next one, the cation transfer from tetragonal to trigonal positions is energetically unfavorable, although it keeps the

TABLE 6. Electric field parameters of some tetragonal and other crystals

Crystal		MC and E[1]	V[2]	ξ[3]	η[4]	a_1[5]	$u=a_3/a_1$	x
TiO_2	α	45.05315	−44.7410	−0.5715	0.8007	4.5929	0.64428	0.3056
	E	282.5011	25.8847	−18.7457	0.5771			
TiO_2	α	44.9729	−44.6666	−1.5513	0.2415	4.5929	0.64428	0.3019
(idealized)	E	281.9979	25.8329	−18.8228	0.6840			
TiO_2	α	45.0541	−44.7325	−0.6412	0.5627	4.59373	0.64395	0.3053
(accurate)	E	282.4560	25.8815	−18.7563	0.5863			
MgF_2	α	11.18855	−22.1115	−0.6869	0.8344	4.623	0.66018	0.31
	E	69.6999	12.7385	−8.7917	0.4281			
MgF_2	α	11.16177	−22.0591	0.6573	0.9017	4.623	0.66018	0.3045
(idealized)	E	69.5331	12.7074	−8.8576	0.5957			
SnO_2	α	44.37777	−42.8444	1.7130	0.1574	4.73727	0.67262	0.3066
(idealized)	E	269.7860	24.6021	−15.9266	0.5263			
RhO_2	α	44.94618	−44.9465	2.6861	0.2998	4.4862	0.68842	0.3092
(idealized)	E	282.5850	25.6998	−17.9531	0.4367			
RuO_2	α	43.94613	−44.8291	2.8010	0.3720	4.4919	0.69160	0.3098
(idealized)	E	281.7556	25.6098	−17.7228	0.4164			
CrO_2	α	44.6529	−46.2538	1.4995	0.9471	4.41	0.65986	0.3044
(idealized)	E	291.6037	26.6472	−20.4263	0.5988			
NbO_2	α	45.4181	−43.3426	2.4173	0.5008	4.77	0.62055	0.2981
(idealized)	E	274.4181	25.2114	−17.8159	0.8130			
$C_{60}A_4$[6]	α	28.9301	15.1320	0.2067	0.0000	11.547	0.92	0.2500
	E	72.1543	−2.9066	−0.6214	0.8139			
$C_{60}A_4$[7]	α	25.6805	15.4509	0.5523	0.0000	11.547	0.92	0.1250
	E	64.0496	−0.5615	−1.8938	0.0286			
$CaCl_2$	α	10.9179	−16.0023	−0.4456	0.1686	6.24[8]	0.67308	0.275
	E	50.3890	9.1922	3.3769	0.7114	4.7311[9]	1.03045	0.325
$La_{2-x}Sr_xCuO_4$[12]	La		−27.9468	−1.7641	0.0000	3.784	1.892	0.183[10]
			+3.8199x	−0.0357x		$\alpha=51.1014$		0.636
	Cu		−27.6449	8.4531	0.0000	+1.2915x		0.367[11]
			−6.0018x	−1.1265x				0.267
	O(apical)		19.2841	1.7356	0.0000			
			−1.3522x	+2.3381x		$E=194.3073$		
						+4.9109x		
	O(plane)		22.1269	5.3429	0.1643+			
			4.0057x	+9.6860x	0.1376x			

[1]The cell energy in eV (per two molecules).
[2]The potential (in V). The first row in each crystal entry refers to cation, the second row to anion.
[3]The main component of EFG tensor (in 10^{20} V/m^2). The first row in each crystal entry refers to cation, the second one to anion.
[4]The asymmetry coefficient of EFG tensor. The first row in each crystal entry refers to cation, the second one to anion.
[5]Geometric parameters: a_1 is the lattice constant, u is the contraction coefficient, and x is a coefficient at the relative distance between cation and anion. In idealized structures of cassiterite type, it is $x=(1+u^2/2)/4$. The lattice constants are taken from the same sources as in Refs. 8 and 43.
[6]The tetragonal structure with tetragonal (T) positions filled in the bases and equatorial plane.
[7]The tetragonal structure with trigonal (I) positions filled in the bases and equatorial plane.
[8]The unit of length; the rest geometric quantities are the relative parameters of the orthorhombic group.
[9]This MC, relative to the closest anion–cation distance, coincides with one calculated in Jonson and Templeton (Ref. 43).
[10]Relative coordinates of the apical oxygen.
[11]Relative coordinates of the La.
[12]The occasional distribution of Sr is modeled by charges $3-x/2$ on La and $2+x$ on Cu.

type of the structure. It is evident from columns 5, 9, and 10 that partial occupation of I positions "induces" EFG in C_{60} sites. Only the complete filling of the whole I set restores the zero gradients (column 12). The first bcc model for superfulleride[6] $C_{60}A_9$, is presented in column 11. The data for bcc superfullerides[39] B_3C_{60}, B_4C_{60}, and B_6C_{60}, doped by alkali earth cations B also can be extracted from Table 8 if the values from columns 4, 6, 8, and 10 for g, ξ, and MC are multiplied by 2, 2, and 4, respectively, and η remains unchanged.

7. Hexagonal Lattices

Consideration of hexagonal lattices will follow the same lines as those of cubic ones. We accept hcp of spheres with radius 1/2 as an ideal structure. That means the following

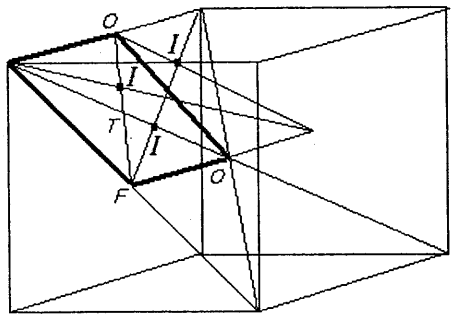

FIG. 7. Positions of trigonal vacancies (I) in the fcc crystallographic cell.

values of lattice parameters: $a_1=1$, $a_2=1$, $a_3=\sqrt{(8/3)}$, $\theta_{12}=120°$, $\theta_{13}=\theta_{23}=90°$. It is convenient to place the origin of the coordinate system between the octagonal vacancies. Then the "atomic" positions have coordinates shown in Table 9. There are two octagonal, four tetragonal, and 14 trigonal (I) vacancies in each cell. There exists a close correspondence between these cavities and their analogs in the case of the fcc lattice. In particular, the radii of similar vacancies are the same as is seen from Table 9. The difference lies only in that the touching fullerene "balls" now belong to the adjacent cells in some cases. As in the fcc lattice, each tetragonal vacancy is surrounded effectively by four trigonal ones (possibly, they are sometimes situated in the neighboring cells as well). However, here there are two special I points which belong simultaneously to two different T vacancies. These specific I points may be filled or unfilled together, independently of all other trigonal vacancies without the violation of the equivalence of all other points. Geometrically, I points are intersections of a straight line connecting adjacent T and O points with the radius of the closest C_{60} sphere perpendicular to this line.

All electrostatics of this lattice are contained in Table 9. The features of MIPs mentioned earlier are also repeated, however; the variety of the potential values is greater. In Table 10, we show the results of calculations for 20 hcp

TABLE 7. Electric field parameters of fcc superfullerides

			O		T		I			
	X	$g(C_{60}^{-X})$	N^1	$-g$	N	$-g$	N^1	$-g$	$\frac{1}{2}\xi^2$	MC
1	4	15.2473	0		0		16	1.0821	181.249	32.6589
2	5	18.7425	4	0.7920	0		16	0.7231	236.175	48.6982
3	5	19.0303	0		4	4.3531	16	1.2536	188.911	52.2593
4	5	19.0303	0		4	−9.5033	16	−2.2105	529.456	38.4029
5	6	22.8132	0		8	−9.2155[3]	16	−2.0391	537.118	62.0741
6	6	22.5254	4	0.5042	4	−9.5033	16	−2.5696	584.382	57.9374
7	6	22.5254	4	0.5042	4	4.5331	16	0.8945	243.837	71.7938
8	7	26.3083	4	0.2164	8	4.6409[4]	16	−2.3982	592.044	85.1036
9	8	30.4947	0		0		32	1.0771	227.233	126.2869
10	9	33.9898	4	−1.9112	0		32	0.7180	282.159	154.8704
11	9	34.2776	0		4	−8.9332	32	1.2485[5]	234.895[5]	147.8484
12	10	37.7727	4	−2.1990	4	−8.9332	32	0.8894[6]	289.821[6]	179.9270
13	10	38.0605	0		8	−8.6454	32	−2.0442	583.102	173.4806
14	11	41.5557	4	−2.4868	8	−8.6454	32	−2.4032	638.028	209.0543
15	2	7.5659	0		4*	7.5659	0			15.1317
16	2	6.9903	4*	6.9903	0		0			13.9805
17	3	11.0610	4	2.9195	4*	7.5659	0			25.6171
18	3	10.7732	4*	6.7025	4	3.7829	0			24.7537
19	4	14.5561	4*	4.0707	8		0			39.5976
20	4	15.1317	0		8*	8.1414	0			46.5463
21	5	18.6268	4	2.3439	8*	8.1414	0			64.0219
22	6	22.1220	4*	5.8391	8*	8.1414	0			88.4878
23	8	30.4947	0		0		16*	2.1643	362498	130.6357
24	9	33.9898	4	−1.9112	0		16*	1.8052	417.424	159.2192
25	9	34.2776	0		4	4.9232	16*	2.3357	370.160	166.0536
26	10	37.4849	4*	1.5839	0		16*	1.4461	472.350	194.7930
27	10	37.7727	4	−2.1990	4	4.9232	16*	1.9766	425.086	198.1322
28	10	38.0605	0		4*	8.7062	16*	2.5072	377.822	209.0374
39	11	41.5557	4	−2.4868	4*	8.7062	16*	2.1481	432.748	244.6111
30	12	45.0508	4*	1.0084	4*	8.7062	16*	1.7890	487.674	287.1751

[1]The number of filled vacancies of suitable type. The asterisk * means that corresponding vacancies are filled by cations of doubled charge.

[2]The dimensionless coefficient at the main component of EFG tensor is ξ. The absence of a suitable column means that $\xi=0$ for all rows. The asymmetry coefficient $\eta=0$ for all cases.

[3]The value for another half of T vacancies is 4.6409.

[4]The value for another half of T vacancies is −9.2155.

[5]The values for another half of I vacancies are −2.2156 and 575.540, respectively.

[6]The values for another half of I vacancies are −2.5747 and 630.366, respectively.

TABLE 8. Electric field parameters of bcc superfullerides

1	2	3	4	5	6	7	8	9	10	11	12
	x	3	3	4	4	6	6	6	6	9	12
C_{60}^{-x}	g	8.8823	8.7943	11.8393	11.7257	17.6766	17.5886	17.7589	17.7589	26.4709	35.5178
	ξ	0	0	39.824	12.145	0	0	28.586	−14.550	0	0
	N^1	6	0	0	0	6	0	0	0	6	0
	$-g$	2.9609				0.4095				−2.1418	
O	ξ	−85.657				316.966				−479.09	
	η	0				0.7817				0	
	N^1	0	6	0	8	6	12	0	0	12	0
	$-g$		2.9325		2.0690	0.2932	1.2359			−1.4034	
T	ξ		33.653		63.041	298.600	92.521			357.468	
	η		0		0.8250	0	0			0	
	N^1	0	0	8	0	0	0	12	12	0	24
	$-g$			−0.0109				1.1562	1.2118		−2.8417
I	ξ			−183.56				140.842	145.082		370.337
	η			0.0603				0.8446	0.7434[2]		0.8827
MC		17.4647	17.5902	23.6567	27.5895	54.0839	56.4735	56.7455	56.9120	111.696	196.056

[1]The number of filled vacancies of a suitable type. The rest of the notation is also the same as in Table 7.
[2]EFG parameters for the second half of occupied I points (inside the cube body) are $\xi=-158.478$ and $\eta=0.8309$.

lattices. In all of them, both atomic positions are filled, and the occupation of the rest of their symmetric points guarantees the equivalence of both "atoms." Note that in some cases (such as lines 7, 11, etc.) it is possible to keep this equivalence when only half of the points from the same class are occupied. In cases such as 8, 10, and 13 only the equivalence between T points surrounded by filled I points and the rest of T points is violated; that is quite natural. These types of data may be useful for the consideration of the doping process. The occupation of trigonal vacancies is compatible with the relative radius of these cavities, if only fullerene spheres fill atomic positions. In the latter case, trigonal cavities are available for some alkali ions. On the other hand, this is in accordance with the recent experimental registration of hexagonal doped fullerite crystals.[46,47]

Nevertheless, it is easy to recognize some known crystals in the first columns of Table 10. The third column contains, in fact, the MC of the NiAs crystal with O positions occupied. The fourth one gives the MC of the wurtzite (ZnS). Indeed, transforming a MC to the closest distance between opposite ions, we obtain $2.680\,267/\sqrt{(8/3)}=1.641\,322$. The fifth one is connected to the idealized CdI_2 crystal (Bozorth) and repeats the data.[25] The sixth column is also of interest. If we assume that CdI_2 is a complete hcp analog of fcc fluorite with metal ions that occupy all atomic positions and halogens that occupy all tetragonal ones, then from the 6th column we obtain an MC in the "chemical" scale: $7.770\,66/\sqrt{(8*3)}=1.586\,18$. The latter is much closer to the value from chemistry textbooks 1.57–1.59[14,52] than the correct value from the 5th column: $6.173\,206/3\sqrt{2}=1.4551$. The reason lies not in the use of the above improperly described structure of the CdI_2 crystal but in the canonization of the very approximate oldest result of Hund[53] quoted in Sherman's review,[54] which made its way from there into other sources.[14] Comparing the lower portion of Table 10 and the suitable parameters of fcc fullerides with the same anion charges (Table 7), we see that generally hcp fullerides have smaller MCs and are less stable. Therefore, fcc fullerides and superfullerides are observed more often. However, the lattice constant is smaller in a hcp as a result of close packing. Therefore, when the whole "I shell" is occupied, i.e., for $x=6$ and $x=7$, hcp fullerides are predicted[40] to be more stable.

As before, all data from Table 10 may be reproduced by means of the MIPs from Table 9. For example, the GPF at Cd and I atoms are $-2g_{AO}=-3.704\,396$ and $2g_{AO}-g_{AA}=2.468\,811$, respectively. Similarly, the MCs of $C_{60}^{-6}A_6$ from the 12th column and $C_{60}^{-7}A_7$ from the 5th column (the lower portion of Table 10) are easily obtained. The attraction of two fullerene anions to the whole family of I charges is $2Q*6(2.285\,234+1.647\,245)=47.189\,748Q$, where integer factors are numbers of interactions. Their mutual repulsion and the mutual repulsion of I charges are $Q^2 1.235\,585$ and $12(3.322\,936+2.392\,315+1.578\,676+1.245\,062)+6(2.285\,234+1.703\,337+1.239\,527)=133.836\,456$, respectively. $\alpha=(6*47.189\,748-36*1.235\,585-133.836\,456)/2=52.410\,486$ in the first case. In the second case, we must add to this attraction the octagonal charges $4Q1.852\,198$, the mutual repulsion of the latter 1.2838, and their repulsion from I charges $6(2.828\,819+1.323\,95)=24.916\,614$, that gives $\alpha=(7*47.189\,748+28*1.852\,198-49*1.235\,585-133.836\,456-1.2838-2*24.916\,614)/2=68.346\,316$. Since specific I^* points are situated on the same "vertical" axis as "atoms" and T points, the asymmetry of EFG for I^* is absent as well as for T points. The results from the 5th column (lower portion) explicitly demonstrate that I^* charges as a result of their position feel doubled repulsion from T charges as compared to the rest of the I charges.

It is necessary to take into account the fact that real crystals deviate from ideal hcp more often than in the case of the fcc lattice. In particular, real geometry of mentioned CdI_2, ZnS as well as ZnO, BeO etc. does not exactly satisfy the

TABLE 9. Madelung interaction potentials of hcp lattice

Points	*A*	*O*	*T*	*I*
A	1.235 59 $r_{1,2}=1$	$g_{1,3}=1.852\ 20$ $=g_{2,4}$	$g_{1,6}=g_{2,7}=2.403\ 05$, $g_{2,6}=g_{1,7}=1.512\ 80$	$g_{1,22}=2.671\ 07$, $g_{2,22}=1.283\ 80$; $g_{1,17}=g_{1,12}=2.285\ 23$, $g_{1,9}=g_{2,17}=1.647\ 25$
O	$r_{1,3}=(\sqrt{2})/2$, $r_{2,4}=(\sqrt{11})/6$	$g_{3,4}=1.283\ 80$ $r_{3,4}=(\sqrt{6})/3$	$g_{4,6}=2.403\ 05$, $g_{3,6}=g_{3,8}=1.400\ 79$	$g_{3,10}=g_{3,9}=2.828\ 82$, $g_{3,21}=g_{4,21}=1.852\ 20$, $g_{3,17}=g_{3,18}=g_{3,15}=g_{3,14}=1.323\ 95$
T	$r_{1,6}=(\sqrt{6})/4$, $r_{2,7}=(\sqrt{38})/4$; $r_{2,6}=5(\sqrt{6})/12$, $r_{1,7}=(\sqrt{6})/4$	$r_{4,6}=(\sqrt{6})/4$; $r_{3,6}=(\sqrt{22})/4$, $r_{3,8}=(\sqrt{102})/12$	$g_{7,8}=g_{5,6}=2.333\ 80$, $g_{5,7}=1.852\ 20$, $g_{6,7}=1.235\ 59$ $r_{7,8}=(\sqrt{6})/2=3r_{5,6}$, $r_{5,7}=(\sqrt{2})/2, r_{6,7}=1$	$g_{5,12}=4.996\ 04$; $g_{5,10}=g_{5,9}=2.080\ 99$; $g_{5,17}=g_{7,14}=1.873\ 30$, $g_{5,16}=g_{5,14}=g_{7,17}=g_{7,14}=1.258\ 63$ $g_{6,22}=g_{8,21}=4.858\ 60$, $g_{7,22}=g_{6,21}=1.400\ 79$
I	$r_{2,22}=(\sqrt{6})/3=r_{1,22}\sqrt{2}$; $r_{1,12}=(\sqrt{6})/3=r_{1,17}\sqrt{2}$; $r_{1,9}=(\sqrt{3})/3$, $r_{2,17}=(\sqrt{11})/3$	$r_{3,10}=(\sqrt{6})/6$, $r_{3,9}=(\sqrt{2})/2$ $=r_{3,21}, r_{4,21}$ $=(\sqrt{66})/6$; $r_{3,17}=(\sqrt{22})/6$, $r_{3,18}=(\sqrt{34})/6$, $r_{3,15}=(\sqrt{38})/6$, $r_{3,14}=5(\sqrt{2})/6$	$r_{5,12}=(\sqrt{6})/12$; $r_{5,10}=(\sqrt{6})/4$, $r_{5,9}=(\sqrt{102})/12$; $r_{5,17}=(\sqrt{38})/12$, $r_{7,14}=(\sqrt{22})/4$, $r_{5,16}=(\sqrt{118})/12$, $r_{5,14}=(\sqrt{166})/12$, $r_{7,17}=5(\sqrt{6})/12$, $r_{7,14}=(\sqrt{102})/12$, $r_{6,22}=(\sqrt{6})/12$, $r_{8,21}=7(\sqrt{6})/12$, $r_{7,22}=(\sqrt{102})/12$, $r_{6,21}=(\sqrt{22})/4$	$g_{9,10=3.322\ 94}$, $g_{10,12}=g_{9,12}=2.392\ 32$, $g_{9,13}=g_{10,19}=2.285\ 23$, $g_{12,17}=g_{9,14}=1.703\ 34$, $g_{12,20}=g_{9,15}=1.578\ 68$, $g_{10,17}=g_{9,17}=1.245\ 06$, $g_{9,21}=g_{14,21}=3.018\ 01$, $g_{10,22}=g_{9,22}$ $=g_{17,21}=g_{18,21}=1.537\ 39$, $g_{10,20}=g_{9,18}=1.239\ 53$, $g_{21,22}=1.235\ 59$ $r_{9,10}=1/3$, $r_{10,12}=(\sqrt{2})/3, r_{9,12}=(\sqrt{5})/3$, $r_{9,13}=1, r_{10,19}=(\sqrt{3})/3$, $r_{12,17}=2(\sqrt{6})/9, r_{9,14}=4(\sqrt{6})/9$, $r_{12,20}=(\sqrt{33})/9, r_{9,15}=(\sqrt{105})/9$, $r_{10,17}=(\sqrt{66})/9, r_{9,17}=(\sqrt{93})/9$, $r_{9,21}=1/3, r_{14,21}=(\sqrt{17})/3$, $r_{10,22}=(\sqrt{5})/3, r_{9,22}=2(\sqrt{2})/3, r_{17,21}$ $=(\sqrt{13})/3, r_{18,21}=4/3$, $r_{10,20}=5(\sqrt{3})/9, r_{9,18}=(\sqrt{129})/9$, $r_{21,22}=1$
Vac. rad	1.0000	$\sqrt{2}-1=0.4142$	0.22474	0.15470
Points' numbers and coordinates	1. 2/3, 1/3, $\frac{1}{2}$ 2. 1/3, 2/3, 0	3. 0, 0, $\frac{1}{4}$ 4. 0, 0, $\frac{3}{4}$	5. 1/3, 2/3, 3/8 6. 1/3, 2/3, 5/8 7. 2/3, 1/3, 1/8 8. 2/3, 1/3, 7/8	9. 7/9, 2/9, 1/6 15. 4/9, 2/9, 5/6 10. 4/9, 2/9, 1/6, 16. 7/9, 5/9, 5/6 11. 7/9, 5/9, 1/6 17. 2/9, 4/9, 2/3 12. 2/9, 4/9, 1/3 18. 2/9, 7/9, 2/3 13. 2/9, 7/9, 1/3 19. 5/9, 7/9, 1/3 14. 7/9, 2/9, 5/6 20. 5/9, 7/9, 2/3 21.* 2/3, 1/3, 0 22.* 1/3, 2/3, 1/2

[a]The upper right part of the table contains all possible MIPs between characteristic points of the hcp elementary cell. The numbers of some typical points are also shown. The lower left portion gives all possible corresponding distances in the symmetric cell. The diagonal cells of the table include both types of parameters. Points' coordinates are given in the elementary cell skew angled coordinate system. The asterisk * denotes two specific trigonal *I* vacancies.

condition $c:a=\sqrt{(8/3)}$. Calculated electrostatic parameters for these crystals are shown in Table 11. They correspond to the real geometry used in Templeton.[43] The necessary geometric parameters are also included in Table 11.

The quantities similar to those of Table 10 for some crystals are placed in the 3rd and 4th columns for convenience of comparison. It is obvious that relatively moderate deviations from the ideal geometry influence the EFG tensor significantly. The MCs found are in complete agreement with those published by Templeton.[43] (if we correct the anion–cation distances for ZnS and SiO_2, which do not correspond to the values of a and c from that paper[43]), confirming again the reliability of this source of MCs.

The results for some oxides of La_2O_3 type included in this table demonstrate the usefulness of the "idealization procedure" for the electrostatic consideration, when the exact geometry is unknown. If we compare the data for real La_2O_3 with those for its possible counterpart of pure hcp type (with both atom sites filled by La ($z=0.25$), two tetragonal (z

TABLE 10. Electric field parameters of hcp superfullerides

1	2	3	4	5	6	7	8	9	10	11	12
	X	1	1	1	2	2	3	4	5	5	6
C_{60}^{-x}	G	2.4688	2.6803	2.4688	5.3605	5.1491	7.8293	10.5486	13.2398	13.4512	16.1814
	ξ	−0.1379	0.2811	−0.1379	0.5621	0.1432	0.4242	−9.1501	11.2216	11.6406	22.157
	N^1	2	0	1		2	2	2	2	0	0
O	$-g$	2.4206		3.7044		2.3211	2.2217	2.2217	0.97604		
	ξ	2.6867		−10.081		−2.9063	−8.4993	−8.4993	−35.567		
	N^1	0	2	0	4	2	4	4	2	4^2	0
T	$-g$		2.6803		2.4101	2.7923	2.5221	0.1786	2.6770	2.2948	
	ξ		−0.2811		27.4966	−6.2930	21.4847	256.593	20.929	54.719	
	N^1	0	0	0	0	0	0	2	6	6	12
	$-g$							−1.6393	1.1798	−0.9221	1.2888
I	ξ							508.939	142.474	356.450	117.763
	η							0	0.2443	0.1175	0.3967
MC		2.444 70	2.680 27	6.173 21	7.770 66	7.705 79	15.3770	21.5671	36.6956	31.0892	52.4105
	X	6	7	7	7	7	8	8	9	9	10
C_{60}^{-x}	G	15.9202	18.8616	18.6502	18.6393	18.9006	21.5419	21.3304	24.1070	24.0497	26.7300
	ξ	11.5027	22.438	22.0190	1.9285	12.582	22.7186	22.3002	22.5807	12.725	13.006
	N^1	2	0	2	2	0	0	2	2	2	2
O	$-g$	0.8766		−0.2696	0.8766			−0.3691	−0.4685	−0.3691	−0.4685
	ξ	−41.160		−62.635	−41.160			−68.228	−73.821	−68.228	−73.821
	N^1	4^3	2	0	4^5	0	4	2	4	2	4
T	$-g$	2.4068	−4.4515		0.0633		−4.7216	−4.3395	−4.6096	−6.6830	−6.9531
	ξ	48.707	−209.98		283.816		−182.20	−215.99	−188.21	19.119	46.896
	N^1	6	12^4	12	8^6	14^7	12	12^8	12	14^9	14
	$-g$	−1.1424	1.2670	1.0685	−1.7653	0.6659	−1.0552	1.0467	−1.2755	0.4238	−1.8984
I	ξ	396.342	126.655	157.491	437.257	159.792	383.512	166.551	423.351	211.426	467.077
	η	0.1111	0.3452	0.3091	0.5255	0.1676	0.1458	0.2753	0.1370	0.1360	0.0851
MC		45.4411	64.1404	68.3463	57.9203	67.7080	78.2804	82.6570	99.3779	101.050	118.146

[1]The number of filled vacancies of a suitable type. The rest of the notation is also the same as in Table 8. The absence of an appropriate row means that $\eta=0$ in all cases.

[2]For the "surrounded" T positions the corresponding parameters are $g=4.6063$ and $\xi=-209.423$.

[3]For the "surrounded" T positions the corresponding parameters are $g=4.4943$ and $\xi=-215.434$.

[4]For I charges which surround occupied T positions the corresponding parameters are $g=1.0394$, $\xi=373.341$, and $\eta=0.1544$.

[5]For the surrounded T positions, the corresponding parameters are $g=6.8378$ and $\xi=19.674$.

[6]For two specific I positions, the corresponding parameters are $g=3.4408$, $\xi=-619.879$, and $\eta=0$. The occupied I points surround T_2 and T_3 positions.

[7]For two specific I positions, the corresponding parameters are $g=0.8838$, $\xi=231.456$, and $\eta=0$.

[8]For I charges which surround occupied T positions the corresponding parameters are $g=1.2537$, $\xi=413.232$, and $\eta=0.1446$.

[9]For I charges which surround occupied T, positions the corresponding parameters are $g=1.8766$, $\xi=455.469$, and $\eta=0.0879$, while for two specific I positions these are $g=2.9379$, $\xi=485.856$, and $\eta=0$.

$=0.625$) and one octagonal ($z=0$) positions occupied by O), we notice that the most essential difference is the increase of nonequivalence of oxygen ions ($g(O_{oct})=20.15$, $g(O_{tet})=19.17$) in the hcp structure. Thus the natural trend in the real crystal is the approaching electric potentials of nonequivalent oxygen ions. Therefore, the oxide with identical potentials of all oxygen ions may be considered "idealized." To reach this goal it is enough to alter z(La) within the last experimental figure: for $z(La)=0.244\,55$ the potentials become $g(O_{oct})=19.960$ V, $g(O_{tet})=19.962$ V, while MC remains almost unchanged, being equal to 40.137. If we postulate this condition for the other oxides too and use the interpolation formula $z=0.018\,3913\ c/a+0.215\,917$, the results placed in Table 11 are obtained. The difference with the data[8] where z values of La were kept for Ce and Pr oxides, is very small and does not influence the conclusions of that paper. This idea may be tested by comparison of potentials in real Nd_2O_3 from the table (whose geometry is measured accurately and differs most significantly from idealized) with the "ideal" ones: −29.758 and 20.509. It should be emphasized that this procedure does not extend onto EFG, remaining different at both oxygen ion types.

The aforementioned doped crystal $C_{60}(P_4)_2$ is an interesting example of not closely packed hexagonal lattice. A small

TABLE 11. Electric field parameters of hexagonal symmetry crystals in real geometry

Crystal		MCs	V^1	ζ^2	E^3	a, A	c/a	z
ZnS[4]	α	10.7153	20.2013	0.1344	40.4025	3.819	1.6355	0.375
Wurtzite	α_R	6.5719	2.6788[5]	0.2599[5]				
ZnO[4]	α	10.8428	24.0241	4.4161	48.0483	3.2495	1.6024	0.345
	α_R	5.9941	2.7107[5]	5.2615[5]				
BeO[4]	α	10.7461	28.6769	2.6762	57.3538	2.698	1.6234	0.365
	α_R	6.3676	2.6865[5]	1.8250[5]				
NiAs	α	10.0455	−19.6142	−2.4141	80.3178	3.602	1.3906	0.25
	α_R	6.7701	20.5447	6.2303				
CdI_2	α	6.2175	−12.7043	−1.8504	21.1155	4.24	1.6168	0.25
	α_R	4.3819	8.4112	−0.0708				
$TiCl_2$	α	6.1270	−14.8262	−3.8262	24.7757	3.561	1.6498	0.25
	α_R	4.3474	9.9495	0.0334				
La_2O_3	α	40.1496	−28.9744	1.1150	146.8369	3.9373	1.5569	0.245
	α_R	24.1787	19.9203	−2.2473	19.9922[6]	−0.9563[6]		0.645[7]
Nd_2O_3	α	40.1435	−29.7923	1.3408	151.0380	3.8272	1.5654	0.2463
	α_R	24.1290	20.2843	−2.2109	20.6884[6]	−1.4351[6]		0.6469[7]
Ce_2O_3	α	40.1096	−29.3150	1.1661	148.5505	3.888	1.5610	0.24463
(idealized)	α_R	24.1663	20.2021	−2.3337	20.2016[6]	−1.0311[6]		0.645[7]
Pr_2O_3	α	40.1359	−29.6170	1.1946	150.0761	3.851	1.5570	0.24455
(idealized)	α_R	24.1785	20.4072	−2.4411	20.4089	−10099		0.645[7]
SiO_2	α	54.5936	−47.9303	−8.1020	470.7359	5.01	1.0918	[8]
	α_R	17.6094[9]	30.5257	40.8143	0.5723[10]	0.0954[11]		
Cr_2O_3	α	62.257	−34.9265	0.9158	1085.77[12]	4.954	2.7420	0.3475
	α_R	24.652[13]	25.3893	−12.370	0.511[11]			0.306[14]

[1]The potential in Volts (if different is not stated). The first row in each crystal entry refers to cation; the second one refers to anion.
[2]The main component of EFG in 10^{20} V/m^2. The asymmetry coefficient is zero unless it is not given explicitly. The first row in each crystal entry refers to cation; the second one refers to anion.
[3]The cell energy in eV (if different is not stated).
[4]All data for cation differ only in sign.
[5]The relative values: $a=1, Q=1$. Relative values are presented for the sake of comparison with the data from Table 10.
[6]The values of V and ζ for oxygen ion in tetragonal position are given for comparison.
[7]The value of z coordinate of tetragonal oxygen. The geometrical parameters are the same as in Torrance (Ref. 8), Templeton (Ref. 43) with the exception of the shortest distances between cation and anion in ZnS and SiO_2. The value 2.339 05 has been used in Jonson and Templeton (Ref. 43) for the former, while 2.3423 corresponds to a and c from that paper, etc.
[8]The rest of the geometric parameters are taken from (Ref. 60) for β quartz.
[9]This value coincides completely with that calculated in Jonson and Templeton (Ref. 43) and differs only by 0.8% from the first result (Ref. 14), which belongs to Hylleraas (Ref. 61).
[10]EFG asymmetry coefficient for Si position.
[11]The EFG asymmetry coefficient for O position.
[12]The hexagonal cell contains six molecules.
[13]This case allows estimating the influence of the accuracy of geometric parameters on the electrostatic quantities. Using rhombic cell with geometric parameters taken from the same source (Ref. 60) gives for $\alpha_R=24.666$. The relative difference of the other quantities is of the same order.
[14]The relative parameters of hexagonal cell for Cr and O, respectively.

charge transfer $(-Q)$ from P_4 molecules to fullerene is noted.[47] Phosphorus molecules in this crystal may be described as elliptic charge distributions placed into octagonal vacancies of this lattice.[47] "Vertical" coordinates of focuses are 0.5 ± 0.081 (in units of c). We can assume that $Q/4$ charges occupy these points and calculate the charge transfer energy. However, we must exclude interactions between focuses of the same molecule. The most convenient tool to do this is MIPs. These are 2.266 72 between C_{60} and the focuses and 2.658 47, 2.553 87 between the focuses of different molecules. Therefore, $\alpha=(Q/4)(Q/4)2.266\,717-(2Q^2/16)\times(2.658\,47+2.553\,87)=1.615\,17Q^2$. This corresponds to the charge transfer energy of $-2.3028Q^2$ (eV), taking into account that $a=c=10.1$ A.

8. Surface Field Parameters Of Ionic Crystals

The method of calculation described in Sec. 2 is especially suitable for the calculation of surface field parameters. To

find a field from a single neutral surface, it is only necessary to omit one summation in Eq. (3). Adding the results for several similar surfaces, we obtain the potentials of a layer, a film, a set of different layers, etc. In the same manner, it is possible to verify that the exact value of the GPF inside the crystal body is created by only 3–4 adjacent planes from each side. For instance, using this method we may calculate that the GPF in NaCl above the Na ion decreases with the increase of the distance from (100) plane as 1.2908, 0.1320, 0.0143, 0.0015, 0.000 17, and 0.000 02 for each quarter of the lattice constant. The contributions to the same constant inside the crystal body are −3.231 08 (from the own plane), −3.498 22 (after addition of the two adjacent planes), and −3.495 09 (after addition of the two next adjacent planes). The next two planes lead to the exact value from Table 1: −3.495 12.

If a neutral plane divides the crystal into two identical halves, it is evident that the surface GPF can be obtained from the GPF of that plane and the GPF of the whole crystal by means of

$$g_{\text{surf}}=(g_{\text{plane}}+g_{\text{body}})/2. \tag{12}$$

The ratio $\gamma=g_{\text{surf}}/g_{\text{bulk}}$ is necessary for determining the surface electronic states of ionic crystals.[55] The interest in surface MCs has, in fact, appeared simultaneously with the introduction of these quantities for the volume materials.[56] However, the number of published results has not increased significantly from that time and yields the amount of data on the volume MCs.

The results of surface MC calculations for some crystals are shown in Table 12. These parameters were obtained directly by summation of contributions from five to six underlying planes and checked by means of Eq. (12). Only in the case of NaCl's surface (100) was there complete agreement with the data.[55,56] The rest of the data for γ[56] (which are more accurate than the data[55]) differ from the values in Table 12 by 0.02–0.04. The difference reaches 0.1 for the data[55] defined as estimated. Perhaps, it is worthwhile to mention that the latter values have been used in real experimental investigations[57] of the shift of x-ray electronic levels in ionic crystals.

The number of neutral surfaces in ionic crystals is even greater than the number of crystals themselves. Therefore, in Table 12 we try only to demonstrate different types of possible situations, which can be met in such calculations, and to make some comparisons with previous works.

The data for crystal layers are also included in Table 12. We define a "monolayer" as a set of equidistant identical crystal planes, which are mutually shifted in any direction and come to take up the same relative positions as in the crystal. The whole crystal can be built of such layers without their mutual displacement. For instance, the monolayer consisting of (010) planes in the NaCl crystal contains three planes, while those corresponding to (210) and (211) planes contain 11 and 19 planes, respectively. The number of planes in a monolayer is usually odd. An even number of planes is an indication of some peculiarities of the given case, such as in the (010) layer of $BaBiO_3$, or in the (101) layer of wurtzite. In the first case, it is evident that the monolayer consists of two different planes: BaO and BiO_2. In the second case, the outer planes are identical, but mutually shifted. Besides, a separate plane divides the crystal into two parts which are on different distances from that plane. Therefore, Eq. (12) cannot be applied here.

The explanations of $\gamma>1$ easily follow from the consideration of how the environment has been changed in the plane's case as compared to the volume's case. The clearest demonstration of this phenomenon is the change of cation potential in I position of $C_{60}^{-4}A_4$. In that case, the closest opposite charges on C_{60}^{-4} from the same cell are removed. This enormous increase has a direct connection with the fulleride's doping ability because the positive potential at the positive ions decreases the cell energy, and to increase the cell energy the alkali ions try to penetrate inside the crystal, where this potential is lower. Thus, the assumption[55] that $\gamma<1$ is valid only for diatomic crystals and only for atomic positions. It follows from this assumption that surface anions are traps for electrons and cations for holes.

The bottom portion of the Table 12 demonstrates the results of "synthesis" of a layer from the neutral planes of different crystals. The TiO_2 and MgF_2 crystals have been used as examples because they have close geometric parameters. In the first case, the MgF_2 plane has been placed between two TiO_2 planes. In the second case, the TiO_2 plane substitutes a similar plane in the same position in the MgF_2 layer. The potential values for infinite mixed crystal, $V(\text{Ti})=-37.758$, $V(\text{Mg})=-28.967$, $V(\text{O})=21.604$, $V(\text{F})=16.920$, which follow from the table, are in reasonable agreement with the results of direct calculation for the middle points of the nine-layer piece of the mixed crystal: $V(\text{Ti})=-37.776$, $V(\text{Mg})=-28.963$, $V(\text{O})=21.610$, $V(\text{F})=16.918$.

The next step of this approach is based on Eqs. (1)–(4). It makes possible the consideration of arbitrary layers and arbitrary surfaces including those defined in Levine[55] as "layer" and "intermediate" ones. These were considered as more difficult for calculations. Their common feature is the nonzero charge of the plane cell. The possibility of removing the restrictive requirement of the planes' neutrality does not, in fact, need a different technique. Indeed, we can apply the third step of the superposition rule Eqs. (4), (5), in the case of a layer with the charged planes as well. However, the line of the infinite system of dipoles for this third step is not directed along the x axis, but along the z axis, while the dipoles themselves continue to have the direction of vector $\mathbf{a}_1$. Therefore, the definition of the $S(p,q,d)$ function is altered here as a result of the difference in the first arguments of functions $F(p,q)$ entering $S(p,q,d)$: the first function depends on x, and the second function depends on $x-x_s$. These arguments enter both parameter p and q in contrast to the former situation, when the altered coordinate (z) entered only q. As a result, the excluded additional logarithmic term must be included here. Note that the third step of superposition may be completely omitted for all neutral planes of the

TABLE 12. The surface electric field parameters of different crystals

			GPF					
					Monolayer			
Crystal	Facet	Position	Plane	Surface	Inner	Outer	N[1]	γ
	(010)	Cl	3.231 08	3.363 10	3.498 22	3.363 08	3	0.962 23
	(110)	Cl	2.662 56	3.078 85	3.621 27	3.072 40	3	0.880 90
NaCl	(210)	Cl	2.779 20	3.137 16	3.495 69	3.137 16	11	0.897 58
	(221)	Cl	1.034 05	2.264 59	3.158 99	2.246 40	7[2]	0.647 93
	(211)	Cl	0.457 97	1.976 05	3.535 32	1.976 31	19	0.565 37
	(110)	Cl	1.773 62	1.904 49	2.050 47	1.904 19	3	0.935 70
CsCl	(110)	O[3]	0.889 45	0.637 77	0.473 06	0.688 08	3	1.413 45
	(110)	I,I'[3]	±0.4898	±0.3389	±0.1787	±0.3391	3	1.802 63
	(110)	H[3]	2.331 17	2.165 58	1.985 68	2.165 89	3	1.082 78
ZnS	(1120)	S	4.479 72	4.920 12	5.447 38	4.917 28	3	0.917 84
wurtzite	(1010)	S	3.511 39	4.106 07	5.500 84	4.114 14	4[4]	0.765 98
ZnS	(110)	S	6.209 81	6.887 83	7.722 21	6.880 77	3	0.910 38
	(110)	O[3], T	±0.8847	±0.7302	±0.4797	±0.7360	3	1.268 46
	(010)	O	6.462 16	6.459 03		6.462 16	2	1.000 48
	(010)	Bi	−11.032	−11.705	[5]	−11.736	2	0.945 63
$BaBiO_3$	(010)	O[3]	−1.8927	−1.2135		−1.1880	2	2.271 06
	(01/20)	O	4.569 43	5.512 67	5.541 28	[6]	2	0.853 90
	(01/20)	Ba	−4.5694	−4.9783	5.007 01		2	0.924 11
	(010)	C_{60}	7.800 51	8.341 42	8.942 80	8.340 20	3	0.939 10
$C_{60}^{-3}A_3$	(010)	A_F	−1.3384	−2.1496	−3.0149	−2.1483	3	0.726 01
	(010)	A_E	−3.2311	−3.0959	−2.9639	−3.0959	3	1.045 65
$C_{60}^{-4}A_4$	(010)	C_{60}	10.0266	10.8761	11.8149	10.8743	3	0.927 55
	(010)	A_P	−1.0837	−1.5764	−2.1120	−1.5754	3	0.761 89
$C_{60}^{-4}A_4$	(010)	C_{60}	9.718 16	10.7787	11.9387	10.7766	3	0.910 42
	(010)	A_I	1.677 36	0.844 13	−0.0574	0.845 63	3	77.36 53
CaF_2	(110)	Ca	−6.2098	−6.8878	−7.7222	−6.8808	3	0.910 40
	(110)	F	3.547 25	3.809 00	4.100 95	3.808 38	3	0.935 70
			Potential (in V)					
TiO_2	(010)	Ti	−33.796	−39.268	−47.069	−39.137	3	0.8777
	(010)	O	18.7677	22.3262	26.7636	22.2738	3	0.8625
MgF_2	(010)	Mg	−16.645	−19.378	−23.173	−19.320	3	0.8764
	(010)	F	9.1160	10.9273	13.1581	10.9030	3	0.8578
$(TiO_2)_2$+	(010)	Ti	−33.539	−35.648	−29.937	−35.597	3	0.9437
MgF_2	(010)	O	18.4990	20.0516	17.2920	20.0299	3	0.9279
$(MgF_2)_2$+	(010)	Mg	−16.770	−22.868	−40.123	−22.736	3	0.7896
TiO_2	(010)	F	9.2495	13.0847	22.5203	13.0308	3	0.7733

[1]The number of planes in the monolayer.
[2]Three monolayers are necessary to obtain the correct surface GPF, and four monolayers are necessary to obtain the correct volume GPF.
[3]Octagonal vacancy; point F in Fig. 2. Other vacancies (I,I' etc.) also correspond to Fig. 2.
[4]Here, the distance between monolayers differs from the distance between the planes inside the layer. This is partly the reason why in this and similar cases a different version of the computer program has been used. The computer calculates the position of the coordinate origin of each plane inside the layer in one version of the program. In the other version these positions are included in the input data. In the latter case, a layer can be constructed of planes taken from different crystals, and "mixed crystals" can be built. Calculation of any entry on the table together with EFG parameters takes less than a second on a PC.
[5]In this case, these are also the outer positions.
[6]In this case, these are also the inner positions.

layer, and the described changed version of the procedure has to be applied only to charged planes.

Summation of logarithmic terms gives rise to a new problem. At first glance, it seems that the above technique can only worsen the series convergence because of the replacement of the summation of the inverse distances by the summation of their logarithms. However, the explicit formulas for the sum of the logarithms can be obtained. To be more specific, let us consider a simple case when all charges are concentrated in two planes: (a_1,a_3), and a parallel plane which intersects lattice vector $\mathbf{a}_2$ at point $Y\mathbf{a}_2$. Then after two stages of the shifting procedure, described in Sec. 2, the charge distribution is reduced to a set of, say, Q charges, situated in all vertices of plane cells in the (a_1,a_3) plane and a similar set of $-Q$ charges, situated in all vertices of the second aforementioned plane. The potential of this system can be found by means of the described method.

Application of Eqs. (1)–(2) allows for the presentation of this potential in the form

$$V(r)=Q(U(p,q)-U(p',q'))/a_3, U$$
$$=4\sum_{n=-\infty}^{\infty}\sum_{l=1}^{\infty}K_0(2\pi l p_n)\cos(2\pi l q_n)$$
$$-\sum_{n=-\infty}^{\infty}\ln p_n^2, \tag{13}$$

where the previous expression of p_n may be modified:

$$p_n^2=(u_{11}u_{22}-u_{12}^2)y^2/u_{11}+u_{11}(x-u_{12}y/u_{11}-n)^2. \tag{14}$$

The presentation of q_n remains the same as in Eq. (2). In the primed quantities, y should be replaced by $y-Y$. The single sum in Eq. (13) can be evaluated together with the similar contribution from $U(p',q')$ by means of the modified Euler product presentation for sine [Gradstein, Ryzhik,[41] Eqs. (1.431) and (1.436)], namely as

$$\sum_{n=-\infty}^{\infty}\ln(((n-a)^2+b^2)/((n-c)^2+d^2))$$
$$=\ln((\sin^2\pi a+\sinh^2\pi b)/(\sin^2\pi c+\sinh^2\pi d)). \tag{15}$$

As a result, the calculation of U becomes very simple:

$$U=4\sum_{n=-\infty}^{\infty}\sum_{l=1}^{\infty}K_0(2\pi l p_n)\cos(2\pi l q_n)$$
$$-\ln\kappa u_{11}(\sin^2\pi(x-u_{12}y/u_{11})+\sinh^2\pi v y), \tag{16}$$

where $v=(\sqrt{u_{11}u_{22}-u_{12}^2})/u_{11}$. The inclusion of the constant $\kappa=(e^C/2\pi)^2$ permits the use of this equation even when the corresponding logarithmic term from U' has all zero arguments (and must be omitted).

It is not difficult to show that "atomic structure" becomes indistinguishable at large distances from planes, and Eq. (16) turns into the standard expression for the potential of charged plane: $U=-2\pi\sigma|y|$ (y is the distance from the plane and σ is the surface charge density).

Our system is transformed into two infinite sets of equidistant parallel lines of opposite linear charge densities $\pm\gamma$ in another limit case when $a_3\to 0$ but $Q/a_3\to\gamma$ remains finite. Then the contribution from the sums disappears. Taking into account the connection between the screw angle and the accompanying Cartesian coordinate system, shown in Fig. 1 (we have interchanged the roles of x and y axes for this purpose), we can see that potential (16) reduces to

$$U=\gamma\ln(\sin^2(\pi\xi/R)+\sinh^2(\pi\eta/R))/$$
$$(\sin^2(\pi\xi'/R)+\sinh^2(\pi\eta'/R)). \tag{17}$$

Here, ξ and η are Cartesian coordinates of the observation point, and R is the distance between the lines. The primed quantities are: $\xi'=\xi-s$, $\eta'=\eta-d$, where s is the shift of the negative charge lines relative to the positive ones along the planes, and d is the distance between the planes.

It is necessary to make a comment before presenting the results of the calculations. As is clear from the considered first limit case, there exists a voltage between opposite sides of any layer containing charged planes. Therefore, at large distances it behaves like a double electric layer. Since we are interested in the "atomic" part of the electric field, it is natural to exclude the influence of the aforementioned uniform field. A model of this procedure is the assumption that the set of layers of the above type is placed between the plates of a charged capacitor. The position of the plates and the value of the capacitor charge are determined from the condition of the field disappearance outside the capacitor.

In particular, let us consider our basic system QL_2. Here, the capacitor charge should be $Q/2$, and the distances of its plates from the frontier charged surfaces for the set of plane layers are $(1/4)a_2$. (We remind you that the distance between charged planes in L_2 will be 1/2 in units of a_2). This guarantees the absence of the field created by the charged planes of the layers outside the capacitor. Note that for an infinite set of layers, i.e., for the solid body, these plates are removed to infinity. In other words, they are, in fact, absent, but this model allows us to obtain the potential of the bulk ionic crystal as the limiting case of the infinite set of layers containing charged planes.

Thus, we shall distinguish three types of potential in layers of the above type: natural potential calculated by means of Eqs. (13) and (16), screened potential, obtained by addition of the capacitor field to the former one, and local potential, i.e., the difference of natural potential and the potential of solid planes with the uniform surface charge density and the same positions as the planes of the initial layer formed of point charges. The screened potential may be presented as the sum of the local potential and the "zigzag" potential which changes linearly between the values $\pm 2\pi Qd(a_2-d)/a_2$ on the charged planes. Table 13 illustrates all these peculiarities. A similar but more complicated picture is observed in other cases since an arbitrary set of layers can be

TABLE 13. Geometric potential factors for L-system layers consisting of charged planes

Face	N^1 Point[2]	Local A	Local Q	Natural A	Natural Q	Screened A	Screened Q
(100)	7^3	−2.749 63	1.652 85	−2.749 63	1.652 85	−2.749 63	1.652 85
(110)	7^3	−2.756 51	1.305 93	−2.756 51	1.305 93	−2.756 51	1.305 93
(001)	1^3	−4.113 77	0.166 57	−0.972 18	3.308 16	−2.542 97	1.737 37
(001)	2^3	−4.106 23	0.170 14	2.176 96	6.453 33	−2.535 43	1.740 94
(001)	3^3	−4.106 21	0.170 15	5.318 56	9.594 93	−2.535 42	1.740 94
(001)	$7^{3,4}$	−4.106 21	0.170 15	17.884 94	22.161 30	−2.535 42	1.740 94
(001)	7^5	−4.312 16	0.089 04	−1.170 57	3.230 63	−2.741 37	1.659 84

[1]Number of layers. The layer planes are parallel to the plane $ABCD$ in Fig. 2.
[2]The point notation corresponds to Fig. 2.
[3]GPF for the points in the first layer.
[4]MCs for the cells of the first layer are 4.212 97, 1.071 37, 2.642 17 for local, natural, and screened cases, respectively.
[5]GPF for the points in the fourth layer. The bulk MC has the same but positive value as GPF for A point.

composed of layers corresponding to several QL_2 systems. From Table 13, it is clear that the local potential reaches its limit value in the first layer after the addition of one or two layers to the initial one just as in the case of neutral planes. Therefore, the parameters of an infinite volume ionic crystal can be evaluated from the data for the middle part of a system with 7–9 layers.

It can also be observed that natural and screened potentials include the field of the charged planes and are changed drastically after the addition of each new layer. The most important conclusion follows from the last row of the table: the values of the screened potential in the central part of the seven layers coincide with the results of direct calculation for the bulk L system by means of Eqs. (9). This argument provides the most convincing support for this approach to the charged plane case. It is evident that for comparison of the volume and surface properties, one should analyze the difference between the data in the last and preceding row of the table.

In particular, the difference of the MCs is independent of the type of the potential used and may be defined as the surface energy: 0.0992, which is of the order of 3.6% of the total cell energy. More generally, the ionic crystal surface energy can be defined as the difference of the total cell electrostatic energy inside the crystal body and on the crystal surface. The possibility of calculating the surface energy demonstrates the usefulness of the concept of the crystal layer. It is more suitable in this respect than the concept of crystal plane.

The neutral layer cell always exists in contrast to the plane cell. Therefore, in order to find the surface property, it is only necessary to calculate in a standard manner the suitable quantity for the cell of the surface layer. Naturally, all data from Table 12 for neutral planes are reproduced in this way. We have included in Table 13 the results for the neutral faces (100) and (110) for the sake of comparison. Obviously GPFs in the neutral case are independent of the potential type. The most interesting feature, which these examples demonstrate, is the possibility of both signs for the surface energy: 2.741 36−2.749 63=−0.0083 and 2.741 36−2.756 51 =−0.0152, while for (001) it was 0.0992. The sign depends merely on the type of interaction of the surface cell with the adjacent cell of the attached layer. The repulsion prevails in the first two cases. Since the effective thickness of the layer is smaller for the (110) face, the absolute value of the surface energy here is greater. At the same time, adjacent cells of (001) attract each other.

Similar peculiarities are observed in real crystals. Therefore, for the sake of brevity, we present analogous results only for the first and central layers of some typical ionic crystals in Table 14 (the data for several traditional cubic lattices are shown in the upper part of the table). The local potential behaves like the potential of a neutral plane; in particular, the influence of adjacent layers fades at the distance of 2–3 lattice constants. From this, it follows that at similar distances outside the crystal body, the natural potential reaches a stationary value. This parameter is given in the ninth column of Table 14. For the same reason, this voltage for the set of several layers is proportional to the number of layers. In particular, this quantity may be zero, as in the case of TiO_2, since this crystal is composed of finite quadrupoles. The data for neutral cases: NaCl (110) and CaF_2 (110) are included for the sake of comparison with Table 12.

The potential in the middle of the screened layer set reproduces the correct bulk value, as is evident from the comparison of the bold figures from the eighth column with the corresponding quantities in Tables 1, 4, and 6. It should be mentioned that EFG is identical for either type of potential, since these differ only in linear terms.

It is also worth emphasizing that in such cases as $YBa_2Cu_3O_7$, there is no way to calculate the surface parameters other than to consider the charged planes since, in this crystal, neutral planes, which divide the crystal onto symmetrical parts, do not exist. It should be mentioned that thin films made from this material were carefully studied experimentally (see e.g. Martovitsky[58]), and surface puckering was discovered. This is in accordance with the positive surface energy of this crystal shown in the last column. The data from the last rows of the table show that the difference in the surface and bulk potentials of this crystal is weaker than in

TABLE 14. Potentials of charged planes in layers of some ionic crystals

Crystal and facet	Position	Local		Natural		Screened		External natural[2]	Surface energy
		1^1	5^1	1^1	5^1	1^1	5^1		
CsCl	Cl	3.614 36	3.606 16	25.605 51	0.464 57	2.043 56	**2.035 36**	3.141 59	−0.077 63
(010)	Cs	−3.753 21	−3.606 16	24.521 12	−0.464 57	−2.182 42	**−2.035 36**		
NaCl	Cl	5.774 10	5.589 53	−31.9250	1.400 73	3.679 71	**3.495 13**	4.188 79	−0.086 09
(111)	Na	−5.577 13	−5.589 53	−34.8987	−1.400 73	−3482 73	**−3.495 13**		
NaCl	Cl	3.078 85	3.495 13	3.078 85	3.495 13	3.078 85	**3.495 13**	0.0	0.353 22
(110)	Cl′[3]	3.558 20	3.495 13	3.558 20	3.495 13	3.558 20	**3.495 13**		
Cu_2O	O	7.957 87	8.047 33	−20.3165	5.905 733	6.387 07	**6.476 53**	3.141 59	0.208 84
(110)	Cu	−1.938 33	−2.212 13	−30.2127	−5.353 72	−3.509 13	**−3.782 93**		
$BaBiO_3$	Bi	−15.1856	−15.5191	41.3631	−9.235 87	−12.0440	**−12.3775**	3.141 59	0.683 84
(110)	O	2.655 19	3.314 31	59.2039	9.597 49	5.796 78	**6.455 90**		
	Ba	−9.027 88	−8.528 79	47.5208	2.245 61	5.886 29	**−5.387 20**		
CaF_2	Ca	−6.887 83	−7.565 84	−6.887 83	−7.565 84	−6.887 83	**−7.565 84**	0.0	1.692 89
(110)	Ca′	−7.644 03	−7.565 84	−7.644 03	−7.565 84	−7.644 03	**−7.565 84**		
	F	3.808 99	4.070 73	3.808 99	4.070 73	3.808 99	**4.070 73**		
	F′	4.085 84	4.070 73	4.085 84	4.070 73	4.085 84	**4.070 73**		
CaF_2	Ca	−10.8695	−10.7075	102.228	1.858 92	−7.727 95	**−7.565 86**	12.566 37	−0.361 47
(010)	Ca[3]	−10.7097	−10.7074	89.8213	−10.7074	−7.568 06	**−7.565 84**		
	F	7.228 73	7.212 32	107.760	7.212 32	4.087 13	**4.070 73**		
	F[3]	7.212 35	7.212 32	95.1769	−5.354 05	4.070 76	**4.070 73**		
TiO_2[4]	Ti	−61.5578	−59.2721	−37.7823	−35.4967	−47.0262	**−44.7406**	0.0	9.298 43
(110)	O	26.6378	35.1285	26.6378	35.1285	17.3939	**25.8846**		
	Ti′	−56.3477	−59.2721	−32.5723	−35.4967	−41.8162	**−44.7406**		
	O′	11.9409	11.3531	35.7163	35.1285	26.4724	**25.8846**		
	O″	34.4226	35.1285	34.4226	35.1285	25.1787	**25.8846**		
"Half "[4,5]	Ti	−55.3142	−52.8794	−31.5388	−29.1040	−40.7827	−38.3479		
TiO_2	O	31.1042	34.1981	31.1042	34.1981	21.8603	24.9542	0.0	1.04312
(110)	Ti′	−54.0968	−52.8794	−30.3214	−29.1040	−39.5653	−38.3479		
	O′	33.8141	34.1981	33.8141	34.1981	24.5702	24.9542		
	Ti(v)	−18.9837	−20.9242	4.791 69	2.8513	−4.4522	−6.3926		
	O(v)	−13.4518	−13.6011	10.3236	10.1743	1.079 73	0.9305		
YBa_2Cu_3	Y	−43.8371	−43.8369	240.758	−43.7516	−33.3367	**−33.3366**		
O_7	O1	16.2681	16.4696	336.342	52.0334	26.6831	**26.8846**		
(001)[4]	Cu1	−37.5373	−40.0810	282.536	−4.5173	−27.1223	**−29.6660**		
	Ba	−21.9962	−21.9275	279.229	−5.2125	−17.3212	**−17.2525**		
	Cu2	−21.4146	−21.4173	255.442	−29.0706	−28.9237	**−28.9264**		
	O2	34.1401	34.1400	301.736	17.2258	18.9137	**18.9135**		
	O3	34.1613	34.1614	301.529	17.0197	18.8210	**18.8212**	35.563 74	3.834 39
	O4	24.2972	24.1808	321.838	37.2114	23.4456	**23.3292**		
	Ba	−21.9275	−21.9275	234.388	−5.2125	−17.2525	**−17.2525**		
	Cu2	−21.4172	−21.4173	234.898	−29.0706	−28.9264	**−28.9264**		
	O2	34.1400	34.1400	284.281	17.2258	18.9135	**18.9135**		
	O3	34.1614	34.1614	284.303	17.0197	18.8211	**18.8212**		
	O4	24.1808	24.1808	273.127	37.2114	23.3292	**23.3292**		

[1]The number of the observation layer. The total number of layers is nine.

[2]The potential outside the crystal body. The shown value is reached at the distance of two lattice constants from the crystal surface and does not change any more. The potential on the other side of the crystal has the same but negative value.

[3]The first ion is situated on the crystal surface while the second similar ion is inside the first (surface) layer. GPF for Na differs only in sign from that for the corresponding Cl.

[4]The potential for these crystals is given in V.

[5]This crystal has the same rectangular cell of the layer as $TiO_2(a_1\sqrt{2},a_1\sqrt{2}/2,a_3)$ but one of the two molecules is removed from the cell. Ti(v) and O(v) correspond to the values for the vacancies that appeared.

the other cases considered. Only potentials of the frontier plane (Cu 1, O 1) and the next one (Ba, O 4) have noticeable changes: in the surface case, the charge transfer from metal to oxygen is facilitated while the properties of (Cu2, O2, O3) plane remain unchanged. This conclusion follows from the consideration of either type of potential.

The model calculation of the "half TiO_2" crystal, in which one TiO_2 molecule is removed, demonstrates the ability of this technique (and the program) to construct (to calculate) crystal properties from the various "building materials." It is clear that if we were to return the removed molecule, we would obtain the initial TiO_2 crystal. Indeed, the sum of ionic and the corresponding vacancy screened potential gives the potentials of Ti and O, respectively, in TiO_2. Simultaneously, this model provides another check on the proposed technique. If we were to rotate the coordinate system 90°, the same crystal would be built on neutral planes, each containing TiO_2 molecules. The corresponding calculation leads to the same bulk potential values 24.9542 for O and −38.3479 for Ti as those shown in column 8 for the "half TiO_2."

The final comment on this treatment of surface properties is that the use of the above technique, is perhaps even more important for quantum mechanical calculations of molecular crystal layers than the ionic ones. The previous "plane" method has allowed dealing only with flat molecular layers[35] formed of plane molecules not deviating from their common plane. For instance, the increment of the frequency dependent hyperpolarizability of triaminotrinitrobenzene has been calculated in this way when these molecules enter a molecular crystal.[59] Now the possibility has arisen to consider layers of arbitrary molecules with any orientation. However, this is another topic.

9. Conclusions

Present calculations allow for the extension of the conclusion drawn in Jonson and Templeton[43] after the first application of the electronic computer (IBM 704) to the calculation of MCs: "the mathematics is not the determining factor in accuracy with which the Madelung constant is known." Now there are no mathematical obstacles to prevent the determination of all electrostatic field parameters of ionic crystals with any necessary accuracy, including EFG and various surface characteristics. The direct use of these parameters is the determination of the cohesive energy of ionic crystals, the alteration of the binding energy of an electron on an ion in crystal as compared to a free one, the calculations of NQR frequencies, etc. Measurements of cohesive energy, x-ray spectra, positions of electronic levels of complex ions in crystal, the band structure, NQR spectra, and so on, use these theoretical predictions as a starting point. Moreover, in the form of MIP the proposed procedures can be applied to quantum calculations of molecular crystals, molecular films, and oriented molecular layers from the first principles. This would require only a transformation of the Coulomb potential into MIP in the current quantum mechanical programs for isolated molecules. The definition of the ionic crystal surface energy is introduced, and it is demonstrated that this quantity may be positive as well as negative. The technique developed generalizes methods of calculation of MC, site potentials, and EFG for an infinite ionic crystal to a real crystal body, restricted by two parallel planes, which are oriented arbitrarily to the crystal axes. All mentioned parameters may be obtained in any crystal layer at the arbitrary depth from the surface including the surface layer. The results of such calculations are demonstrated.

10. Acknowledgment

The author is highly indebted to Sue Tashlitsky for her help in preparation of the manuscript.

11. References

[1] J. B. Torrance, P. Lacorro, C. Asavaroengchai, and R. M. Metzger, J. Solid State Chem. **90**, 168 (1991).
[2] M. J. O'Keeffe, J. Solid State Chem. **85**, 108 (1991).
[3] R. M. Fleming, M. J. Rosseinsky, A. P. Ramirez, D. W. Murphy, J. C. Tulley, R. C. Haddon, T. Siegrist, R. Tycko, S. H. Glarum, P. Marsh, G. Dabbagh S. M. Zahurak, A. V. Makhija, and C. Hampton, Nature(London) **352**, 701 (1991).
[4] J. Li, H.-L. Liu, and J. Ladik, Chem. Phys. Lett. **230**, 414 (1994).
[5] F. J. Adrian, Phys. Rev. B **38**, 2426 (1988).
[6] M. M. Mestechkin and G. E. Whyman, J. Mol. Struct. **283**, 269 (1993).
[7] M. M. Mestechkin and G. E. Whyman, Mol. Mater. C **8**, 161 (1996).
[8] J. B. Torrance, P. Lacorre, C. Asavaroengchai, and R. M. Metzger, Physica C **182**, 351 (1991).
[9] E. Madelung, Z. Phys. **19**, 524 (1918).
[10] M. Born and M. Geoppert-Mayer, *Dinamicke Gittertheorie der Kristalle Handbuch Physik* (Aufl. Berlin, 1933), B24/2.
[11] M. Born, Z. Phys. **7**, 124 (1921).
[12] P. P. Evald, Ann. Phys. L (Leipzig) **64**, 253 (1921).
[13] H. M. Evjen, Phys. Rev. **39**, 675 (1932).
[14] *Landoldt–Bornstein 1, Atom-und Molekularphysik 4. Kristalle* (Springer Berlin, 1955).
[15] *Handbook of Chemistry and Physics*, 55th–80th eds. (Chemical Rubber Corp., Boca Raton, FL, 1978–1999).
[16] M. P. Tosi, Solid State Phys. **16**, 1 (1964).
[17] Ch. Kittel, *Introduction to Solid State Physics*, 7th ed. (Wiley, New York, 1996).
[18] A. Huag, *Theoretical Solid State Physics* (Pergamon, New York, 1972).
[19] P. P. Pavinskiy, *Introduction to Solid State Theory* (LGU, Leningrad, 1979) (in Russian).
[20] F. J. Adrian, Phys. Rev. B **37**, 2326 (1988).
[21] J. P. Dahl, Phys. Chem. Solids **26**, 33 (1965).
[22] F. Y. Hajj, J. Chem. Phys. **56**, 891 (1972).
[23] W. N. Kleber, Ib. Min. Geol. Paleont. A **75**, 72 (1939).
[24] M. M. Mestechkin and L. S. Gutyrya, J. Phys.: Condens. Matter **5**, 6683 (1993).
[25] P. Hartman, Acta Cryst. **11**, 365 (1958).
[26] J. Sakamoto, J. Chem. Phys. **28**, 164 (1958).
[27] W. Kukhtin and O. V. Shramko, Phys. Lett. A **156**, 257 (1991).
[28] R. M. Metzger, J. Chem. Phys. **64**, 2069 (1976).
[29] R. M. Metzger, J. Chem. Phys. **57**, 1870 (1972).
[30] G. Hummer, Chem. Phys. Lett. **235**, 297 (1995).
[31] D. York and W. Jang, J. Chem. Phys. **101**, 3298 (1994).
[32] A. Hunt and M. Pollak, Philos. Mag. B **53**, 353 (1986).
[33] M. M. Mestechkin, J. Phys.: Condens. Matter **6**, 1677 (1994).
[34] M. M. Mestechkin, J. Phys.: Condens. Matter **6**, 611 (1995); **6**, 3371 (1995).
[35] M. M. Mestechkin, J. Phys.: Condens. Matter **9**, 157 (1997).
[36] *Handbook of Mathematical Functions*, edited by M. Abramovitz and I. A. Stegun (Dover, New York, 1972).

[37] F. Hund, Z. Phys. **94**, 11 (1935).
[38] G. C. Benson and F. van Zeggeren, J. Chem. Phys. **26**, 1083 (1957).
[39] M. M. Mestechkin and G. E. Whyman, Theor. Exp. Khim. **32**, 13 (1996).
[40] M. M. Mestechkin and G. E. Whyman, J. Struct. Khim. **38**, 1122 (1997).
[41] I. S. Gradstein and I. M. Ryzhik, *Tables of Integrals, Sums, Series, and Products* (Fizmatgiz, Moscow, 1972).
[42] J. E. Lennard-Jones and B. M. Dent, Philos. Mag. **3**, 1204 (1927).
[43] Q. C. Jonson and D. H. Templeton, J. Chem. Phys. **34**, 2004 (1961).
[44] M. Mestechkin, G. Whyman, and G. Klimko, Mol. Phys. **82**, 1079 (1994).
[45] C. Ambrosh-Droxl, P. Blaha, and K. Schwarz, Phys. Rev. B **42**, 205(1990), **44**, 5141(1991).
[46] T. Yildrim, O. Zhou, and J. E. Fisher, Nature(London) **360**, 568 (1992).
[47] L. Q. Jiang and B. E. Koel, Chem. Phys. Lett. **223**, 69 (1994).
[48] A. R. Kortan, N. Kopylov, and E. Ozdas, Chem. Phys. Lett. **223**, 501 (1994).
[49] A. R. Kortan, N. Kopylov, and S. H. Glarum, Nature(London) **355**, 529 (1992).
[50] J. L. De Boer, S. van Smaalen, and V. Petricek, Chem. Phys. Lett. **219**, 469 (1994).
[51] I. W. Locke, A. D. Darwish, H. W. Kroto, K. Pressides, R. Taylor, and D. R. Walton, Chem. Phys. Lett. **225**, 186 (1994).
[52] G. V. Bokiy, *Crystalochemistry* (Science, Moscow, 1971).
[53] F. Hund, Z. Phys. **34**, 833 (1925).
[54] J. Sherman, Chem. Rev. **11**, 93 (1932).
[55] J. D. Levine and P. Mark, Phys. Rev. **144**, 751 (1966).
[56] K. F. Herzfeld, Z. Phys. Chem. (Frankfurt) **105**, 329 (1923).
[57] J. P. H. Citrin and T. D. Thomas, J. Chem. Phys. **57**, 4446 (1972).
[58] V. P. Martovitsky and V. V. Rodin, Physica C **182**, 269 (1991).
[59] M. M. Mestechkin, Opt. Spectrosc. **87**, 714 (1996).
[60] R. W. G. Wyckoff, *Crystal Structures*, sec. Ed. (interscience, New York, 1963), Vol. 1, p. 313.
[61] E. A. Hylleraas, Z. Phys. **44**, 871 (1927).